

# **Regulation of Autophagy by mTORC1 and ULK1**

**Peter Doubleday**

**A dissertation for the degree of Master of Philosophy**

**Cardiff University Institute of Cancer and Genetics**

(Student number: 1358762)

**2015**

## CONTENTS

	<b>Pages: 65</b>
<b>Abstract</b>	<b>4</b>
<b>Declaration</b>	<b>4</b>
<b>Acknowledgements</b>	<b>5</b>
<b>Abbreviations</b>	<b>5</b>
<b>List of Figures</b>	<b>6</b>
<b>List of Tables</b>	<b>6</b>
<b>Supplementary Figures</b>	<b>7</b>
<b>1. Introduction</b>	<b>8</b>
<b>1.1 Autophagy in mouse models and cancers</b>	<b>9</b>
<b>1.2 Autophagy mediated by the serine/threonine kinase ULK1</b>	<b>10</b>
<b>1.3 ULK1 mutations and clinical findings</b>	<b>11</b>
<b>1.4 Downstream targets and regulation of autophagy</b>	<b>12</b>
<b>1.5 FLCN, and Birt Hogg Dubé Syndrome—connecting autophagy and disease</b>	<b>13</b>
<b>2. Methods</b>	<b>15</b>
<b>2.1 Antibodies, plasmids and biochemicals</b>	<b>15</b>
<b>2.2 Cell Culture, transfections and immunoprecipitations</b>	<b>15</b>
<b>2.3 Luciferase reporter assays</b>	<b>15</b>
<b>2.4 Western blotting and <i>in vitro</i> kinase assays</b>	<b>15</b>
<b>2.5 Peptide Preparation for Mass Spectrometry</b>	<b>16</b>
<b>2.6 Mass Spectrometry</b>	<b>17</b>
<b>2.7 Bioinformatics</b>	<b>18</b>
<b>3. Results</b>	<b>19</b>
<b>ULK1 biology</b>	<b>19</b>
<b>3.1 ULK1 pull-downs and purification strategy</b>	<b>19</b>

<b>3.2 Identification of novel ULK1 binding partners</b>	<b>19</b>
<b>3.3 ULK1 phosphorylation targets and quantitative proteomics</b>	<b>22</b>
<b>3.4 Inhibitor validation <i>in vitro</i> and <i>in vivo</i></b>	<b>23</b>
<b>3.5 Temporal initiation of autophagy and ULK1 activity and workflow</b>	<b>25</b>
<b>3.6 Quantitative results</b>	<b>26</b>
<b>FLCN biology</b>	<b>29</b>
<b>3.7 Identification of novel FLCN binding partners and validation <i>in vivo</i></b>	<b>29</b>
<b>3.8 Identification of FLCN phosphorylation sites and modulation by pharmacological inhibition</b>	<b>30</b>
<b>3.9 FLCN-interactome related to disease progression and common disease phenotypes</b>	<b>34</b>
<b>3.10 FLCN as a regulator of biology in the nucleus and primary cilia</b>	<b>36</b>
<b>4. Discussion</b>	<b>42</b>
<b>5. Summary of research highlights</b>	<b>47</b>
<b>6. References</b>	<b>48</b>
<b>7. Supplemental Figures</b>	<b>53</b>
<b>8. Supplemental Tables</b>	<b>digital format</b>

## **Abstract**

Macroautophagy is a catabolic cellular process responsible for bulk degradation of proteins. Largely conserved from yeast to mammals, the initiating steps of autophagy and key signalling proteins governing the complex biological process have been initially characterised. However, very little is known of one critical protein kinase, ULK1, which is thought to govern the induction of autophagy. ULK1 is regulated by two upstream kinases, via energy sensing through AMPK and nutrient sensing through mTORC1. While several studies have identified ULK1 binding partners in cells, the list of functional interactions remains limited. Further, as an enzyme, the targets of ULK1 and the possibility of a consensus phosphorylation motif remains largely unknown. Herein, using a phosphoproteomic screen and purification approaches, we identify new ULK1 protein interactions and ULK1-mediated phosphorylation events. A novel ULK1 kinase inhibitor is also initially characterised, which potently blocks ULK1 phosphotransfer to downstream substrates and itself, and autophagosomal maturation in mammalian cells. Furthermore, examining a known ULK1 binding partner, FLCN, we explore novel molecular aspects of a rare genetic disease, Birt-Hogg-Dubé syndrome and its connection as a ciliopathy.

## **Declaration**

I, Peter Doubleday, declare that the work on which this thesis is based is my original work—except where acknowledgements indicate otherwise. This work has not been submitted in any other form for another degree and published and unpublished work by others is included in the list of references if not acknowledged in the body of the work.

## **Acknowledgements**

I would like to first thank Dr Tee and his laboratory for welcoming me to Wales and for giving me the chance to explore my intellectual curiosities, make connections, learn to be an independent thinker, and understand what a rainy day in Cardiff is all about. I am quite certain that my time in Cardiff and throughout the UK will be the foundation, not only for my continued academic success, but also for seeing complex problems through a unique lens. I would like to thank my previous mentors, specifically Dr Bryan Ballif, for all of his continued support, input on projects and guidance. I would also like to acknowledge Dr James Murray for kindly providing the kinase inhibitor and images of its validation in comparison to Wortmannin. Moreover, the work of Elaine Dunlop has been essential and she has provided Western blot evidence for the validation of interaction between FLCN and DNA-PKc (among other targets which continue to emerge). Third, none of this work would have been possible without the US-UK Fulbright Commission and their dedication to promoting cross-cultural understanding and opportunities to give an ignorant American a true taste of the UK. Finally, to my family—thank you for the continued support and letting me go explore where life takes me.

## **Abbreviations**

**MeCN-** Acetonitrile

**TFA-** Trifluoroacetic acid

**SILAC-** Stable isotope labeling in cell culture

**SCX-IMAC-** Strong cation exchange - immobilized metal affinity chromatography

**LC-MS/MS-** Liquid chromatography mass spectrometry/ mass spectrometry

**BLaST-** Basic logarithmic alignment search tool

**BHD-** Birt Hogg Dubé syndrome

**PtdIns(3)P-** Phosphatidylinositol-3-phosphate

**HEK293-** Human embryonic kidney 293 cell line

**HK2-** Human cortical kidney cell line

**U2OS-** U2 osteosarcoma cell line

**FDR-** False-discovery rate

**pS/T-####-** phospho-serine/threonine- site number

## List of Figures

**Figure 1.** Identification and validation of novel ULK1 Substrates

**Figure 2.** ClustALW2 multiple sequence alignment highlights disparity between yeast atg1 and human ULK1 phosphorylation sites

**Figure 3.** QG000052 potentially inhibits ULK autophosphorylation and kinase activity towards known substrates in vitro and in vivo

**Figure 4.** SILAC-based workflow to identify ULK1-mediated phosphoproteomic changes

**Figure 5.** Bivariate density analysis plotting the measured mass accuracy of the precursor phosphopeptide ions (in ppm) with their  $\text{Log}_2(\text{Treated}/\text{Untreated})$  SILAC ratios

**Figure 6.** FLCN is heavily phosphorylated at proline-directed serine residues

**Figure 7.** Gene Ontology enrichment identifies FLCN to have roles in transport and translation

**Figure 8.** Validation of novel endogenous FLCN interactions and relationship to Birt Hogg Dubé Syndrome disease progression

## List of Tables

**Supplemental Table 1.** Peptides and proteins identified from V5-ULK1 pull-down and mass spectrometry analysis

**Supplemental Table 2.** Peptides and proteins identified from GST-ULK1 pull downs and mass spectrometry analysis

**Supplemental Table 3.** ULK1-binding proteins identified as early endosomal components by bioinformatics enrichment

**Supplemental Table 4.** Identification and quantification of peptides identified by SILAC following ULK1 inhibition

**Supplemental Table 5.** Peptides and proteins identified by interacting-protein mass spectrometry (IP-MS) following GST-FLCN pull-down

**Supplemental Table 6.** Gene list for enriched biological processes identified from FLCN interacting proteins.

**Supplemental Table 7.** Gene list for enriched protein domains (INTERPRO) of FLCN binding proteins

**Supplemental Table 8.** FLCN tryptic peptide identification and quantification by chemical labeling and mass spectrometry after pharmacological inhibition

**Supplemental Table 9.** FLCN phosphopeptide identification from non-quantitative experiments from an in-gel digest of GST-FLCN and identification on an LTQ mass spectrometer.

**Supplemental Table 10.** Identification of TIP41 and FLCN complex component FNIP1 and FNIP2 phosphorylation with ULK1

## **Supplementary Figures**

**Supplemental Figure S1.** Quantification of chemically labelled, phosphorylated FLCN peptides under pharmacological inhibitor treatment

**Supplemental Figure S2.** Luciferase assay measurements to detect the role of FLCN mutation in NF- $\kappa$ B and TGF- $\beta$  signalling response

**Supplemental Figure S3.** Multiple sequence alignment of FLCN and DEN1A and DEN1B highlights DENN-like domain in FLCN

**Supplemental Figure S4.** Identification of FNIP1, FNIP2 and TIP41 phosphorylation sites

## 1. Introduction

Macroautophagy (herein now referred to as autophagy) is an ancient catabolic, cellular process responsible for bulk degradation of dysfunctional proteins and organelles. First coined in 1963, by the Nobel Laureate Christian de Duve, autophagy is characterized by the formation of double-membrane vesicles, called autophagosomes, and their subsequent fusion to lysosomal bodies to provide the cell with greater nutrient availability particularly during fasting or nutrient-deprived conditions. As a distinct pathway from the proteosomal turnover of ubiquitinated, unstable proteins, autophagy-mediated lysosomal turnover has the ability to degrade stable proteins, pathogens (xenophagy) and whole organelles such as mitochondria (mitophagy). Much of the early understanding on autophagy came from work in yeast. Through unbiased yeast autophagy screens the initial network of proteins and biomolecules responsible for autophagy induction grew significantly. This early work led to the discovery of human orthologues and an initial large-scale study shedding light onto the network organization of mammalian autophagy [1].

Autophagy is a highly orchestrated, dynamic process that is modulated at several points. Autophagy initiation is regulated by a core set of five protein complexes. Classically these can be defined as (1) the UNC-51-like kinase (ULK1) complex, made of ULK1, ATG13L, ATG101, and FIP200, (2) the VPS34 kinase complex, composed of VPS34 (PI3KIII), VPS15 (PIK3R4), Beclin1 and ATG14 or UVRAG, as well as (3) PtdIns(3)P binding proteins such as DFCP1 and WIPI1 and (4) the ubiquitin-like conjugation system of ATG5-12 and ATG16L. Furthermore (5), microtubule associated protein 1-light chain (LC3) and related ATG8-family protein phosphatidylethanolamine conjugation via the ATG5-12-16L system and mATG9-positive membranes is required for canonical autophagy [2]. Conjugation occurs through the action of ATG4, a cysteine protease, which cleaves the C-terminus of ATG8 family proteins, including LC3, GABARAP, GABARAPL1 and GABARAPL2 [3]. Further, ATG7, an E1-like activating enzyme activates ATG12 for conjugation to ATG5, allowing for proper membrane targeting of LC3 [4]. The list of known kinases and proteins regulating autophagy continues to expand. A comprehensive review on autophagy initiation by KL Guan reveals a highly regulated multifaceted process that still requires further delineation [2]. See **Box 1** for a schematic diagram of autoautophagy initiation.



## 1.1 Autophagy in mouse models and cancers

Genetic studies in mouse have underlined the importance of autophagy network genes in proper embryonic development and more recently in cancer progression. Indeed, mice deficient in both *Ulk1* and *Ulk2* die within 24 h of birth. Moreover a bi-allelic deletion of either *Atg5* or *Atg7* in mice results in offspring that cannot survive past the first day following birth. Without *Ulk1* or *Ulk2*, *Atg5* or *Atg7*, mice are unable to appropriately maintain energetic homeostasis during the first fasting state when maternal nutrition is no longer available [5]. Lethality during this first period of perinatal life demonstrates a systematic failure to recycle primary metabolites in an autophagic-dependent manner.

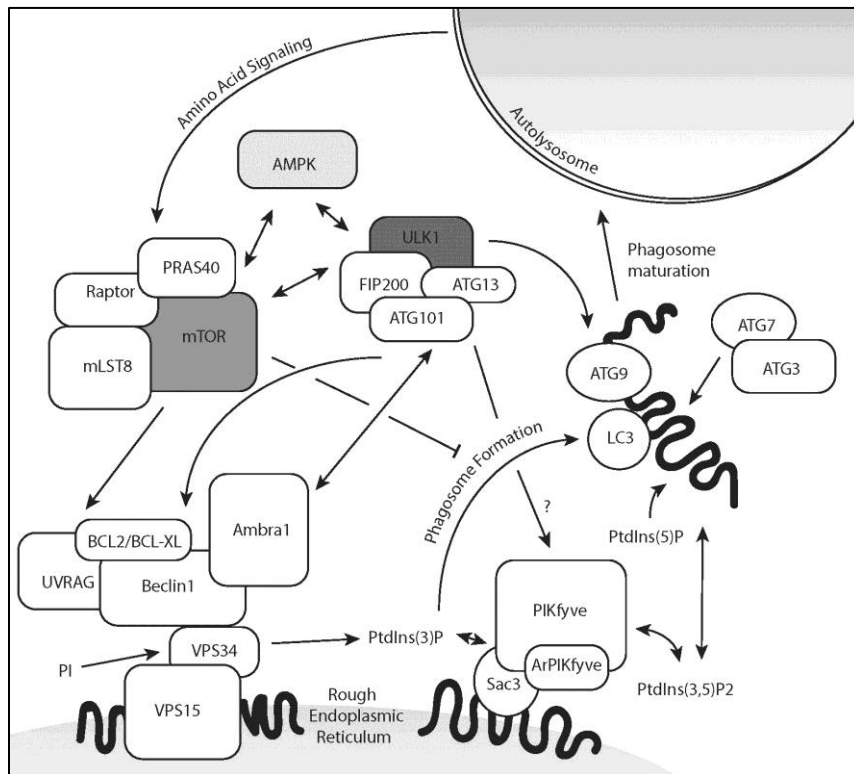
Interestingly, mice deficient in *Ulk1/2*, *Atg5* or *Atg7* all exhibit relatively consistent pathological phenotypes. Lung development is severely limited in knock-out mice, and alveolar space in the lung is significantly reduced. Additionally, high glycogen levels in the lung were observed, although surfactant producing lamellar bodies were unchanged and overall, the ability to regulate membrane trafficking was largely impaired. The developmental mechanism governing *Ulk1/2* and *Atg5/7* early post-natal death evidently requires further examination, yet present studies indicate ULK1 and autophagy are essential for life and proper development [5].

Little is known regarding autophagy in the context of cancer although autophagy has been suggested to act as both a promoter and a suppressor of tumourigenesis. Evidence of its suppressive activity comes from gene deletion studies in mice. These studies demonstrated that loss of autophagy promotes the formation of multiple types of benign liver tumours [6]. In contrast, blocking autophagy inhibits tumour growth in advanced tumours, suggesting that targeting autophagy could have a potential therapeutic role in metastatic disease [7]. In mouse models of pancreatic ductal adenocarcinoma, autophagy promotes tumour growth and progression [8]. Tumours exhibit elevated autophagy as marked by the accumulation of GFP-LC3 puncta. Moreover, when autophagy is genetically ablated, either through deletion of *Atg5* or *Atg7*, a greater level of tumour initiation is noted, yet lesions were impaired from progressing to an invasive cancer type. The connection between autophagy and cancer progression has been examined in other cancer types. For instance, in breast cancer patients, high-levels of ULK1 expression correlate to a reduced likelihood of event-free survival [9]. Furthermore, autophagy

appears to have the shared dual role in mouse models of lung cancer that are seen in pancreatic cancer models [10].

## 1.2 Autophagy mediated by the serine/threonine kinase ULK1

One major gap in our understanding of autophagy is the list of known substrates for the serine/threonine protein kinase ULK1. The ULK kinase family shares little homology with any of the other 257 human protein kinases. ULK1 puncta formation is noted as one of the earliest events in autophagosome formation. Although the consensus phosphorylation motif of the yeast orthologue of ULK1, ATG1, was identified through the generation of a novel synthetic peptide library and proteomic screen [11]; a gapped BLAST and alignment reveals no overlap to human orthologues of the proteins reported outside of ULK1 itself. Moreover, the suggestion that mATG9 is a physiological target of ULK1 in early autophagy remains somewhat unexplained as ATG9-positive membranes do not form into phagophores and have not been seen to associate with early autophagic proteins such as ULK1. Instead, ATG9 is largely thought to participate at recycling endosomes and the endoplasmic reticulum, a late stage in autophagy [12].



**Box 1. Interplay between amino acid signalling, energy sensing and autophagy.** ULK1 phosphorylates AMPK, Raptor, Beclin1, ATG9 and possibly PIKfyve or Sac3. The VPS34 complex responds to both mTORC1 and ULK1 for the respective repression or initiation of lipid kinase activity. Ambra1 is phosphorylated by mTOR but also stabilizes ULK1. The ATG7 E-3 ligase allows for the acylation of LC3.

The PIKfyve lipid kinase complex converts PtdIns(3)P into the lower abundance phospholipid, PtdIns(3,5)P<sub>2</sub>, which in turn can be converted into PtdIns(5)P. ATG9 is phosphorylated by ULK1 to initiate autophagy.

ULK1 mediates its physiological function through its three-domain structure and has a kinase domain, a species-variable signalling sensor domain, called a PAS domain, and a conserved C-terminal domain and in humans there are four related ULK kinases [13, 14]. ULK1 and ULK2 are the most closely related of the family and have been studied to the greatest extent thus far. While the two kinases share a high degree of similarity at the molecular level, they have significantly distinct areas of their kinase domain conferring a possibly nuanced autophagy-specific function. Between the large and small lobes of the kinase domain resides a large loop, largely distinct to the ULK family of kinases. Only the Sgk, Wee1, Mlk, Clk and JAK families of kinases have a similar structural fold. This loop, although seen across the ULK family, is a noted area of distinction between the primary sequence of ULK1 and ULK2, suggesting that there could be ULK1-specific mechanisms that govern autophagy, which ULK2 is not readily privileged to participate in. However, it is likely that this difference underlies nuanced kinetic and thermodynamic differences which dictate functional output [15].

### **1.3 ULK1 mutations and clinical findings**

Unfortunately, there have been few reported clinical perturbations of ULK1 conferring altered phenotypes to gain true biological insight. Indeed, the Sanger Institute's Catalog of Somatic Mutations in Cancer (COSMIC, <http://cancer.sanger.ac.uk/cancergenome/projects/cosmic/>) identified fewer than 200 mutations in ULK1 out of over 20,000 somatic tumour samples. While insight from the clinic remains limited, mutagenesis studies have readily probed structure-function relationships of the ULK1 complex. Kinase-inactive ULK1 generated via mutagenesis of lysine-to-isoleucine (K48I) exhibit reduced kinase activity. In cell culture, K48I-ULK1 cells exhibit lower levels of LC3-lipidation relative to control under serum starvation [16]. From the recently identified kinase domain crystal structure of ULK1, this K48I mutation should severely disrupt kinase activity while not interfering with higher ordered structural conformation. The recent structural elucidation of the ULK1 kinase domain demonstrates that mutating this K48 residue directly interferes with the ATP-binding coordination site, where this residue lies proximal to the interlobe-loop. Mutation to this interlobe-loop is unlikely to manifest major

structural changes as it is largely unstructured, while it is thought to confer a more ordered structure when ULK1 is part of larger kinase complex with Atg13 and FIP200 [15].

#### **1.4. Downstream targets and regulation of autophagy**

The suggested importance of ULK1 has arisen from the requirement of its orthologue in yeast in addition to functional studies in mammalian cell culture. Known as Atg1 in *S. Cerevisiae*, ULK1 has been studied as a target of growth signalling through the mammalian target of rapamycin complex 1 (mTORC1, now more commonly referred to as mechanistic target of rapamycin complex 1) and energy sensing via AMP-dependent protein kinase (AMPK). Under serum or nutrient-deplete conditions, ULK1 is activated by direct phosphorylation by AMPK at serine-555 and serine-467 [17]. Additionally, AMPK-dependent phosphorylation of ULK1 at serine-317 and serine-777 is required for ULK1 activation in response to glucose starvation. Loss of AMPK or the loss of AMPK-phosphorylation sites in ULK1 or ULK2 mimics loss of ULK under nutrient-limited conditions [18, 19]. Related to input from AMPK, under serum-replete conditions ULK1 activity is antagonized by mTORC1-mediated phosphorylation at serine-757, and serine-473. While the exact structural changes propagated by these phosphorylation events remain undetermined, ULK1 kinase activity is significantly decreased and its interaction with AMPK is significantly disrupted [18]. mTORC1 also phosphorylates AMBRA1 directly at serine-51 as a secondary mechanism to inhibit ULK1 ubiquitination and stability. AMBRA1-mediated lysine-63 ubiquitination via the E3 ubiquitin ligase, TRAF6, stabilizes and aids the self-association of ULK1 [20].

In addition to receiving functional input from mTORC1 and AMPK, ULK1 also negatively feeds back onto these kinases, serving a reciprocal regulatory role. ULK1 and ULK2 directly phosphorylate the mTORC1 component, Raptor, at multiple sites preventing substrate interaction with Raptor and sequential phosphorylation of these mTORC1 substrates [21]. Moreover, ULK1 mediates the phosphorylation of all three AMPK subunits to negatively regulate its activity, which consequently leads to down regulation of autophagy [22]. Overall, these reciprocal regulatory mechanisms allow for fine-tuned signalling between three, multi-protein kinase complexes and for the proper regulation of growth, autophagy and energy-sensing signalling.

Downstream of mTORC1 and AMPK, ULK1 functions to regulate VPS34 at the budding omegasome and regulates this protein's ability to produce low abundance, signalling phospholipid phosphatidyl-inositol 3-phosphate [PtdIns(3)P]. Mechanistically, ULK1 phosphorylates a 51kDa protein, Beclin1, the yeast orthologue of ATG6, as part of the VPS34 lipid kinase complex. Phosphorylation of serine-15 on Beclin1 is conserved in *C. elegans* and is required for the complete induction of autophagy [23]. Beclin1 is also phosphorylated by AMPK at serine-93 and serine-96, demonstrating multiple modes of its post-translational regulation. ULK1 is further stabilized by AMBRA1, a WD40 protein and E3-ligase interacting protein, linking the ULK complex to the VPS34/Beclin1 complex, although ULK1 interaction with AMBRA1 appears to be unchanged with regards to nutrient availability [20] [24].

### **1.5 FLCN, and Birt Hogg Dubé Syndrome—connecting autophagy and disease**

A lesser-studied target of ULK1 phosphorylation is the protein folliculin (FLCN). Germline mutations in FLCN are responsible for Birt-Hogg-Dubé (BHD) syndrome, an autosomal, dominantly-inherited genetic tumour syndrome, characterized by the development of fibrofolliculomas, lung cysts, renal neoplasia and increased cancer risk. The syndrome presents in approximately 20% of patients as renal neoplasia, and often presents at late developmental stages, or is only identified at the development of renal cancers [25-27]. On a molecular level, the gene product responsible for the pathology, FLCN, can act as a classic tumour suppressor; however the exact molecular function of the protein, and how its functional loss manifests disease, remains largely unknown. The protein has no classic motifs or domains; however, truncation mutations have been reported in patients with renal cell carcinoma (RCC) and recent work in cells has identified FLCN as a mediator of mTORC1 and growth signalling as well as being an AMPK substrate. Previous work has demonstrated that targeted loss of FLCN can result in activation or suppression of mTORC1 signalling in a context-dependent manner [25, 28]. While FLCN has been reported to act as a GTPase activating protein (GAP) towards RagC/D GTPases, directly linking FLCN to nutrient sensing and mTORC1 signalling, FLCN has also been reported to act as Rag guanine exchange factor (GEF) [29, 30]. UOK257 cells depleted of FLCN undergo metabolic transformation driven by AMPK, yielding PGC1 $\alpha$ -mediated mitochondrial biogenesis. Moreover, loss of FLCN increases reactive oxygen species (ROS) production, and increases Hypoxia Inducible Factor (HIF) 1 $\alpha$  and 2 $\alpha$ -regulated gene expression, including the up-regulation of vascular endothelial growth factor-A (VEGF-A) to increase

vasculature, an increasingly targeted protein for treating renal cancers and reducing the angiogenic potential and metastasis of tumours [31, 32]. While FLCN has been shown to interact with cell structural elements including tight junctions through an interaction with Plakophilin-4 to regulate RhoA signalling [33] and at the base of cilia [34] no report to date has taken a proteomic approach to identify FLCN binding partners. However, there is a very recent link between ULK1 and FLCN as a new potential substrate. The FLCN complex is regulated by ULK1, and moreover, autophagy is impaired in tumours associated with BHD [21].

## **2. Methods**

### **2.1 Antibodies, plasmids and biochemicals**

Anti-FLCN antibodies were provided by Dr Arnim Pause, McGill University, Canada. Anti- $\beta$ -actin, -ULK1, -pS555-ULK1, -pS467-ULK1, -pS757-ULK1, -pS172-AMPK, -AMPK antibodies were purchased from Cell Signaling Technology, Danvers, Mass, USA. Anti-Pikfyve (PIP5KIII) antibody was purchased from Santa Cruz Biotechnology. Anti-V5 antibodies were provided by Life Technologies and anti-LC3 antibodies were sourced from Nanotools, Teningen, Germany. Flag (clone: M2) and anti-V5 were obtained from Sigma-Aldrich as well as formic acid solution, acetonitrile, trifluoroacetic acid, Phos-Select IMAC resin. The ULK1-inhibitor, QG000052, and pS30-Becn1 antibody was a kind gift of Dr. James Murray, Trinity College Dublin. Radio-labelled ATP was sourced from Elmer Perkins, Waltham Mass, USA. Full-length ULK1, ATG13, BECN1, FLCN, were cloned in-line with GST in a pCMV promoted vector, or purchased through Addgene, and validated by sequencing prior to use. The vector to myr-FLAG-PIP5KIII was purchased through Addgene. BHD-shRNA was generated using Mission shRNA constructs (purchased from Sigma-Aldrich Company Ltd.).

### **2.2 Cell Culture, transfections and immunoprecipitations**

UOK257, HK2 and HEK293 cells were cultured at 21% oxygen, 5% CO<sub>2</sub> in Dulbecco's modified Eagle's medium (DMEM) supplemented with 10% (v/v) fetal calf serum, 100 U/ml penicillin and 100 mg/ml streptomycin (Gibco, Paisley, UK). Cells underwent starvation either in Krebs Ringer Buffer (135mM NaCl, 5mM KCl, 1mM MgSO<sub>4</sub>, 0.4mM K<sub>2</sub>HPO<sub>4</sub>, 20mM HEPES, pH7.4), Hanks Balanced Salt Solution (Gibco), or remained in DMEM. Transfections were performed with JetPEI reagent according to the manufacturer's protocol (Polyplus, New York). To immunoprecipitate proteins from whole cell lysates, 2.5 $\mu$ L of primary antibody was added to 500 $\mu$ g of clarified protein in lysis buffer and rocked overnight at 4°C. To each sample, 30 $\mu$ L of a 50% slurry of protein-G sepharose was added and allowed to rock for at least 45 minutes at 4°C. Immune complexes were subsequently spun down by centrifugation for 4

minutes at 2000 x g at 4°C and washed four times in lysis buffer prior. Proteins were eluted with the addition of SDS-PAGE sample buffer and boiling at 95°C prior to loading in pre-cast or in-house made SDS-PAGE gels. GST-containing constructs were rocked overnight in 15µL of a 50% slurry of glutathione-sepharose. Bound complexes were washed in PBS and free GST was added at 1mg/mL in 50mM Tris HCl, pH8, to elute bound proteins.

### **2.3 Luciferase reporter assays**

HK2 cells deficient in FLCN through shRNA knockdown were plated on 96-well plates. Luciferase reporter constructs SBE4 (pGL4.48[*luc2P*/SBE/Hygro]) and NF-κB (pGL4.32[*luc2P*/NF-κB-RE/Hygro]) (Promega, Madison, Wisconsin) and a renilla-luciferase transfection control were co-transfected with an equimolar amount of pcDNA3 or cDNA to wild-type and mutant HA-FLCN constructs. To stimulate reporter activity TGF-β was added to 1ng/mL and reactions incubated for 6 hours prior to fluorescence visualization on a plate reader.

### **2.4 Western blotting and *in vitro* kinase assays**

Cells were washed and then lysed from plates using lysis buffer (20mM Tris, 135mM NaCl, 5% (v/v) glycerol, 50mM NaF and 0.1% (v/v) triton X-100, pH 7.6 supplemented with complete mini protease inhibitor cocktail (Roche Diagnostics Ltd. Burgess Hill, UK) at 4°C. After centrifugation at 17,000 x g for 10min at 4°C samples were prepared in 4X NuPAGE sample buffer (Invitrogen, Paisley, UK) with 25 mM DTT and boiled at 70°C for 10 min. Proteins were separated by electrophoresis using the NuPAGE gel system (Invitrogen) and transferred to polyvinylidene difluoride membranes (Millipore, Watford, UK), blocked in 5% (w/v) dry milk powder/Tris-buffered saline 0.1% (v/v) tween, then probed using the required primary antibody and horseradish peroxidase-conjugated secondary antibody in Tris-buffered saline Tween. Proteins were visualized using Enhanced Chemiluminescent solution and X-ray film (both from GE Healthcare, Buckinghamshire, UK). Unless otherwise stated, Western blots were conducted in biological duplicate.

To perform *in vitro* kinase assays, proteins were purified following overexpression in HEK293 cells. Kinase-substrate reaction mixtures were incubated with radiolabeled ATP for 10 minutes and quenched with SDS-PAGE sample buffer. Kinase assay experiments were conducted in biological triplicate.

### **2.5 Peptide Preparation for Mass Spectrometry**



NuPAGE gels (Invitrogen) used in mass spectrometry analyses were stained directly with Coomassie blue, destained with ddH<sub>2</sub>O, and gel bands were subjected to in-gel tryptic digestion, as previously described (Ballif et al., 2006).

For experiments using stable-isotope labelling by amino acids in cell culture (SILAC [35]), HEK293 cells were grown for at least one week in DMEM deficient in L-arginine and L-lysine (Cambridge Isotope Laboratories, Inc., Andover, MA), but supplemented with 10% dialyzed fetal bovine serum (Hyclone); 50 U/ml penicillin and 50 mg/ml streptomycin (Invitrogen); and either 73 mg/L unlabeled L-lysine and 42 mg/L unlabeled L-arginine, or 73 mg/L 13C6-L-lysine and 42 mg/L 13C6-, 15N4-L-arginine (Cambridge Isotope Laboratories, Inc.). 15cm<sup>2</sup> plates of labelled HEK293 cells were washed and starved for 10 min in Krebs Ringer Buffer. Heavy labelled plates were supplemented with ULK-inhibitor at 10µM. Cells were lysed in lysis buffer 20mM Tris, 135mM NaCl, 5% (v/v) glycerol, 50mM NaF and 0.1% (v/v) triton X-100, pH 7.6 supplemented with complete mini protease inhibitor cocktail (Roche Diagnostics Ltd. Burgess Hill, UK) at 4°C, and snap frozen. An aliquot of each sample was taken for western blotting and Bradford Assays to normalize protein levels.

Following protein normalization, heavy- and light-labeled lysates were combined for 2 biological replicates and resuspended in ice-cold urea lysis buffer (7.99 M urea, 100 mM NaCl, 25 mM Tris pH8.0, 25 mM NaF, 10 mM Na<sub>4</sub>P<sub>2</sub>O<sub>7</sub>, 1 mM Na<sub>3</sub>VO<sub>4</sub>, 50 mM β-glycerophosphate, 1 mM PMSF, 1 mM leupeptin and 1 mM pepstatin). Lysates were sonicated for 3x 1 min intervals at 4°C in a sonicating water bath at 4°C. Insoluble debris was then spun down by centrifugation for 30 min at 15000 x g. DTT was added to 5 mM and the clarified lysate was incubated at 56°C for 40 min. Samples were then reduced with 14 mM iodoacetamide for 1 h in the dark, quenched with DTT to a final solution concentration of 10mM. Samples were then diluted at 1:4 in 25 mM TRIS pH8.0, reducing the urea concentration below 1.6M. Proteins were digested with the addition of sequencing-grade modified trypsin (Promega, Madison, Wisconsin) at 1:100 overnight at 37°C. Following digestion, trypsin was pH-inactivated with trifluoroacetic acid (TFA) to 0.4%. Cellular debris was then removed from the digest via centrifugation at 4000 x g for 20 min at 4°C. The supernatant from biological replicates was desalted on Waters tC18 columns (pre-conditioned by wetting with 100% acetonitrile (MeCN), equilibrated with 0.1% TFA, and eluted in 40% MeCN/ 0.1% TFA), and dried via lyophilization prior to fractionation and phospho-peptide enrichment.

Labelled peptides were subjected to strong-cation exchange (SCX) coupled to immobilized-metal affinity chromatography (IMAC). Briefly, dried peptides were resuspended in SCX buffer A (7mM  $\text{KH}_2\text{PO}_4$  pH2.65, 30% MeCN) and applied to a polySULFOETHYL A solid phase extraction column (PolyLC Inc, Columbia, MD) pre-equilibrated with a blank run of 80% MeCN, water, followed by SCX buffer A for over 30 min. Peptides were fractionally eluted with 6ml fractions of SCX solvent B (7mM  $\text{KH}_2\text{PO}_4$  pH2.65, 30% MeCN, 350mM KCl) adjusted with SCX solvent A to the following concentrations of KCl: 0, 4, 8, 12, 25, 90 and 250mM. Peptides were frozen at  $-80^\circ\text{C}$ , lyophilized, and then desalted on tC18 columns and dried as previously described.

Peptides from each SCX fraction were re-suspended in 100 $\mu\text{l}$  of 40% MeCN/25 mM formic acid (FA) and 40 $\mu\text{l}$  of a 50% slurry of Phoselect IMAC resin (SIGMA) and then vigorously shaken for 1hr at room temperature. An additional 50 $\mu\text{l}$  of re-suspension buffer was added to each fraction, and samples were loaded onto home-made crimped, 200 $\mu\text{l}$  gel-loading tips. Flow-through was collected and re-applied to the IMAC resin 3 times prior to washing twice with 120 $\mu\text{l}$  re-suspension buffer. Phosphopeptides were eluted with 50mM  $\text{K}_2\text{HPO}_4$  pH10, and pH neutralized with 10% FA. Peptides were spun to dryness.

## 2.6 Mass Spectrometry

Peptides from SILAC and pull-down studied were resuspended in 2.5% MeCN/ 2.5% FA and loaded for nano-scale microcapillary LC-MS/MS in an LTQ Orbitrap Discovery mass spectrometer (Thermo Scientific), fitted to a Finnigan Nanospray II electrospray ionization source, an MS Pump Plus HPLC pump and a Thermo Micro AS autosampler (Thermo Scientific). Peptides were separated on an increasing gradient of 99.0% MeCN and 0.15% FA (Solvent B) from 15 to 60 min on a 100 $\mu\text{m}$  internal diameter, in-house prepared 13cm long C18 reverse phase resin (MagicC18Q, Michrom Bioresources, Auburn, CA) with a needle tip diameter of  $\sim 5\mu\text{m}$ .

Initial peptide mass identification and quantification was conducted with an MS1 full scan followed by 10 MS/MS scans in a data-dependent fashion. Peptides were identified using the SEQUEST and MASCOT algorithm (Thermo Electron Version 27 Revision 12) (Eng et al., 1994) ([www.matrixscience.com](http://www.matrixscience.com)) against the human international protein index (IPI) database (Human IPI v6.60.fasta) in a target-decoy approach [36], allowing for phosphorylation of serine, threonine or tyrosine (+79.96633 Da), oxidized methionine (+15.99429 Da),

carbamidomethylated cysteine (+57.02146 Da). For SILAC studies, searches also required differential labelling of lysine (+8.014198 Da) or arginine (+10.008268 Da) and for reductive amination chemical labelling studies, searches required addition of dimethylation (+28.0313) and allowed for differential mass addition of deuterium.

## **2.7 Bioinformatics**

MS runs were initially filtered below a 0.5% peptide-level false discovery rate using an automated linear discriminant analysis weighted by Xcorr, Cn, MS2 ion intensity, missed tryptic cleavages, adjusted precursor PPM and peptide length. The Ascore algorithm was employed to confidently assess phosphorylation site localization on a given peptide based on probabilistic likelihood as described previously [37]. Phosphopeptides were required to have a minimum Ascore of 3, correlating to greater than 80% confidence in the localization of a particular phosphorylation site. The resultant non-quantitative, quantitative, and phospho-specific datasets each had estimated false discovery rate (FDR) below 1%. The DAVID bioinformatics software resource and manual, informed filtering strategies were used to examine protein lists and identify enriched protein categories, gene ontologies and biological processes.

## **3. Results**

### **3.1 ULK1 pull-downs and purification strategy**

Identifying interacting partners of ULK1 has remained fairly elusive. Low protein expression levels, viability of cells over-expressing the kinase, and the temporal dynamics of autophagy have all contributed to a limited understanding of the kinase. Therefore, prior to examining ULK1 interactions, we first optimized transfection and immuno-affinity enrichment strategies. As ULK1-mediated autophagy is thought to occur as early as 15 min following complete withdrawal of nutrients [38], several time points and ULK1 constructs were examined to judge relative levels of ULK1 that could be purified. To enrich for ULK1 *in vivo*, 90% confluent 25cm plates of HEK293 cells were transfected with plasmids to express GST-ULK1 or the kinase-inactive mutant, GST-ULK1<sup>K48I</sup>, and were starved in Krebs's Ringer Buffer (KRB) for 18h. ULK1 binding partners were resolved by SDS-PAGE following GST purification and

subsequent wash steps (**Figure 1a**). In addition to GST-ULK1, untagged and V5-ULK1 was examined by immunoaffinity enrichment; however, these enrichments were observed to purify significantly less ULK1 and had greater non-specific binding as judged by background bands seen in the control lane (**Figure 1b**, *Supplemental Table S1, S2*). While a high degree of background was identified through immunoaffinity enrichment, a greater number of unique bands were also identified. Therefore, both GST and V5-tagged protein interacting bands were excised and subjected to protein identification by mass spectrometry.

### **3.2 Identification of novel ULK1 binding partners**

Following separation by SDS-PAGE, control, wild-type and K48I kinase-inactive ULK1 mutant lanes of the gels were excised and examined by mass spectrometry. After peptides and proteins were identified, a cut-off to only include proteins identified by more than one peptide was used to exclude possible contaminating proteins. Some validated ULK1 binding partners, including AMPK subunits, were only identified by one peptide in the K48I pull-down. While this set cut-off excludes likely *bona fide* ULK1 interacting partners, it also significantly reduces the rate of false positive identifications.

A greater amount of total GST-ULK1 was purified from cells compared to V5-ULK1, yet a similar number of interacting partners were identified by this purification method in total. Filtering peptide identifications below a 2% FDR, we identified 194 ULK1 peptides from GST-WT-ULK1 pull-down, and 82 peptides from GST-KI-ULK1 pull-down. Several hundred proteins were identified as GST-WT and GST-KI-ULK1 interacting proteins; however, many of these are likely contaminants, including keratin proteins (*Supplemental Table S2, S3*).

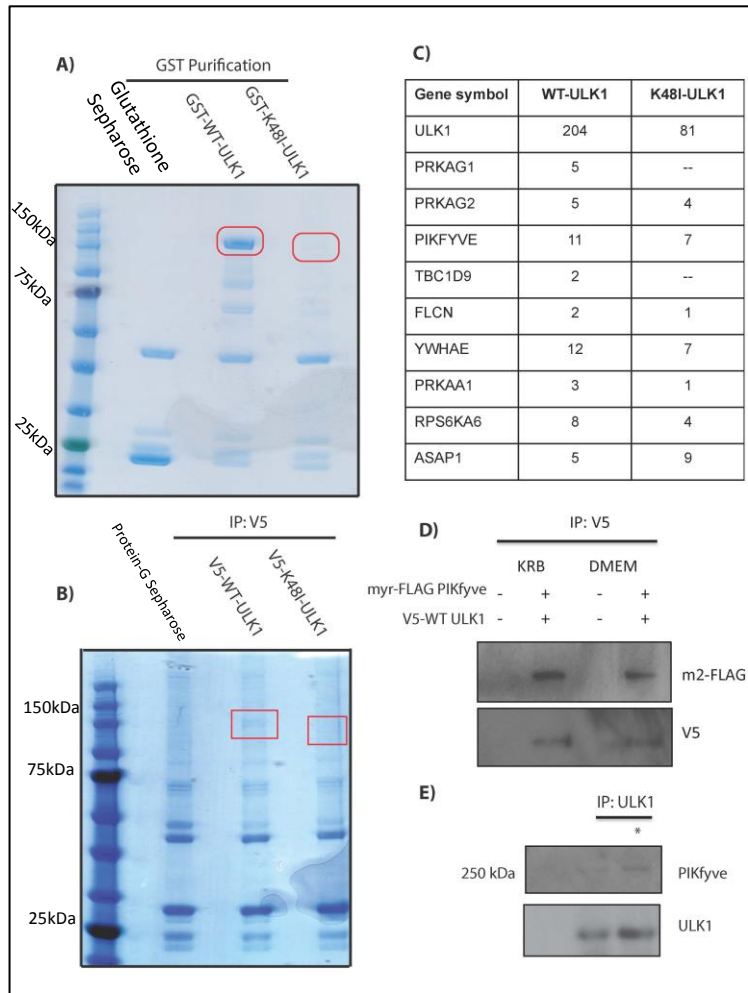


## Figure 1. Identification and validation of novel ULK1 Substrates

**A)** HEK293t cells were transfected transiently with vectors to pCDNA3 alone or with pCDNA3 containing GST-WT- or GST-K48I-ULK1 respectively. Following transfection, cells were starved in Krebs Ringer Buffer for 18hrs prior to lysis. Overexpressed ULK1 and its binding partners were captured by immunoaffinity enrichment separated and visualized following SDS-PAGE and coomassie stain. **B)** Control (IgG alone) and anti-V5 pull-down lanes were excised and protein bands were identified by mass spectrometry, as was done in A. **C)** The top biologically relevant ULK1 interacting partners are given. The entire gene list of ULK1 binding partners can be found in *Supplemental Table 1*.

**D)** V5-WT-ULK1 and FLAG-PIKfyve were co-expressed in HEK293t cells and incubated in either Krebs Ringer Buffer or DMEM. The V5 tag was immunoprecipitated from lysate and pull-downs were blotted for with antibodies against Flag and V5 epitopes. **E)** To further confirm ULK1 binding to PIKfyve, endogenous ULK1 was immunoprecipitated from HEK293t cells using a Santa Cruz Biotechnology antibody (F4) or a Cell signalling antibody\* (D8H5). Following pull-down by SDS-PAGE, endogenous PIKfyve and ULK1 protein levels were then probed for by Western blot.

Indeed, a control pull-down of GST alone identified contaminants, where high levels of keratin and known contaminants such as trypsin were found. To get around contamination and discover more possible biologically relevant ULK1 interactions, we next looked at proteins that associated with V5-ULK1. From this purification a total of 201 ULK1 peptides were identified at an FDR of 2%. In total, 315 proteins were identified as potential ULK1 binding proteins by greater than 3 total peptides, although these proteins remain to be validated by traditional approaches (*Supplemental Table S1*). Expert bioinformatics work and manual interrogation with

prior knowledge of autophagy and endosomal biology is critical for selecting proteins having a high probability of *bona fide* interactions with ULK1.

In addition to known ULK1 substrates such as AMPK (PRKAA) subunits PRKAG1, PRKAG2, FLCN, FIP200, ATG101 (C12orf44), and SYNGAP1, we identified previously unreported substrates which likely participate in various aspects of autophagy, including PIKfyve (PIP5K3), a lipid-binding phosphoinositide kinase responsible for enzymatically turning PtdIns3P to PtdIns(3,5)P2 and PtdIns(5)P with the adapter proteins, Sac3 and ArPIKfyve, also identified in our screen. We also identified ASAP1, an ArfGAP with an SH3 domain, and a number of proteins that participate in early endosomal biology including TBC1D9, a RabGAP (*Supplemental Table S3*). Another early endosomal protein which could play a hand in the regulation of autophagy that we identified in our screen is LYST, the lysosomal trafficking regulator protein, which is thought to be responsible for packing materials into lysosomes [39]. The LYST protein also plays a role in autophagosome maturation, whereby loss of LYST results in compromised immune signalling and oversized autophagosomes [40]. Moreover we identified VPS26, VPS33, and VPS54, involved in retrograde transport from endosomes to the trans-Golgi and endolysosomal transport [41, 42]. Through the identification of all of these candidate proteins, it is likely that ULK1 has a hand in fine-tuning the response of vacuole dynamics and endosomal biology to a greater extent than once thought.

The ArfGAP, ASAP1, functions at the budding primary cilia to regulate receptor targeting. As a GTPase activating protein, ASAP1 binds to and serves as a scaffold for the Rab8/Rabin8 complex, responsible for initial vacuole formation in ciliogenesis. This process is largely analogous to the requirement of small G-proteins in autophagy and may illustrate an evolutionary mechanism by which ULK1 functions upstream of vacuole formation and extension (Figure 1C, *Supplemental Table S1*) [43-45]. Interestingly, ULK1 substrates that have been identified as targets of its kinase activity, such a Beclin1, were found only as minor binding partners in our screen (*Supplemental Table S1*).

We also identified substrates that have no acknowledged role in autophagy including RSK4 (RPS6KA6), which suggests further roles for ULK1 outside of its canonical pathway. RSK4 is a 90-kDa serine/threonine kinase of the ribosomal s6 kinase family (RSK), which is constitutively active in most cell types [46] (*Supplemental Table S1*). Unlike the rest of the RSK family of protein kinases, RSK4 is thought to participate in growth factor independent pathways.

A 2005 paper identified several phosphorylation sites on RSK4, one of which was serine-232 that may be an ULK1 site due to the fact that the yeast Atg1 consensus motif closely matches this phosphorylation site. Additionally, distinct from the other phosphorylation sites identified in this report, serine-232 displayed a nearly inverse pattern of regulation compared to the other sites identified [46].

Although a number of the targets identified by proteomic methods could be functionally interrogated, PIKfyve was selected because it was a top scoring binding partner identified in wild-type and kinase-inhibited ULK1 screens and we identified its binding partner ArPIKfyve (VAC14), to a lesser extent. Additional pull-downs with GST-tagged ULK1 also identified PIKfyve (data not shown). Mechanistically, PIKfyve takes the product of the ULK1-regulated VPS34 complex, PtdIns(3)P and adds a phosphate to create another, less abundant second messenger, PtdIns(3,5)P<sub>2</sub> [47]. The exact role of ULK1 association with PIKfyve is still unknown; however, we find a greater association with wild-type ULK1 to PIKfyve under nutrient limited conditions than in nutrient-replete conditions, suggesting it has a functional role mediated by ULK1 activity (**Figure 1d**). In addition to using over-expressing constructs of ULK1, we also analysed binding of endogenous proteins. We observed that endogenously purified PIKfyve bound to ULK1 in HEK293 cells, solidifying the interaction as a real, *in vivo* candidate for functional characterization (**Figure 1e**).

### 3.3 ULK1 phosphorylation targets and quantitative proteomics

A recent study in yeast identified Atg1 phosphorylation sites by screening a peptide library and using mass spectrometry following incubation with the kinase to determine linear-motif substrate specificity [11]. They reported the preferred phosphorylation motif of Atg1 as LxxSxYxP, and validated this substrate specificity with several yeast proteins and human Beclin1. However, an independent analysis of the human orthologues identified through BLAST and subjected to a sequence alignment with the ClustalW2 program (<http://www.ebi.ac.uk/Tools/msa/clustalw2/>), reveals that only ULK1 at a novel site (517) has a residue which could be phosphorylated out of the candidate yeast protein identified in this study (**Figure 2**). The rest of the yeast proteins remain distinct from human orthologues in their sequence similarity and possible, modified sites. Although this disparate result is somewhat surprising due to the assumed and previously reported level of evolutionary conservation in autophagy, it is at least partially supported by the wide variety of ULK1 sites reported [48]. However this comparative analysis raises the question of

whether a unique human ULK1 phosphorylation motif exists, and how similar ULK1 mechanisms are between species with regards to the conservation of autophagy-associated proteins. Therefore, to probe this question and look for human ULK1 substrates, we looked to identify ULK1-mediated phosphoproteomic changes using quantitative mass spectrometry and a novel ULK inhibitor.



**Figure 2. ClustALW2 multiple sequence alignment highlights disparity between yeast atg1 and human ULK1 phosphorylation sites**

Uniprot accessions from high confidence phosphorylation sites identified by Papinski et al 2014 were used to identify orthologous human proteins through a gapped BLAST search (<http://blast.ncbi.nlm.nih.gov>). The gene identified in this study is given in lowercase lettering, with yeast phosphosite number provided, followed by the corresponding human gene symbol and aligned sequence. Orthologous protein sequences were then compared to identify conserved phosphorylation sites or motif overlaps using a multiple sequence alignment with ClustalW2 (<http://www.ebi.ac.uk/Tools/msa/clustalw2>).

### 3.4 Inhibitor validation *in vitro* and *in vivo*

Many previous studies have employed similar inhibitory mechanisms and peptide libraries or quantitative proteomics to identify consensus kinase motifs. One example is the use of rapamycin and torin-1 as pharmacological inhibitors of mTOR in a quantitative phosphoproteomic workflow to identify the mTOR kinase motif [49]. Analogous to this previous study, we ventured to use a novel inhibitor of ULK1, QG000052, to examine ULK kinase-dependent modifications



*in vivo*. As the ULK1 inhibitor used in this study has not yet been published and characterised, we first endeavoured to validate its effectiveness *in vivo*. Prior to attempting to inhibit ULK1 in a large-scale screen, we initially validated the ULK1 inhibitor, through *in vitro* kinase assays and by western blot. To generate substrates, GST-tagged ATG13, ULK1 and BECN1 were grown and purified from HEK293t cells. By incubating ULK1 in the presence of QG000052 *in vitro*, ULK1 autophosphorylation and phosphorylation of the validated human targets of ULK1, ATG13 and BECN1, were significantly reduced relative to uninhibited ULK1 kinase. 5 $\mu$ M QG000052 treatment resulted in 20% kinase activity of ULK1 relative to the control, demonstrating the potency of the inhibitor (**Figure 3a**). Interestingly a site on BECN1, serine-30, does not seem to be significantly affected by ULK1 treatment nor inhibition, although total BECN1 phosphorylation is significantly reduced by QG000052 treatment. This is likely due to changes in the known ULK1 phosphorylation site on BECN1, serine-15 [23].

Next we evaluated the inhibitor in the context of the functional ULK1 complex. Following immuno-precipitation of ULK1 from HEK293 cells treated with QG000052 in full media (DMEM) or in Krebs Ringer Buffer for 1h, ULK1, FIP200 and ATG13 were probed for by western blot. Relative to control conditions, the inhibitor did not significantly disrupt the association (**Figure 3b**). To further examine ULK1-mediated changes upon inhibition, live-cell imaging was performed on GFP-WIP1 transiently transfected U2OS cells (courtesy of the Murray laboratory). The WIP1 construct was used as it binds to PtdIns(3)P by virtue of its FYVE domain to create discrete puncta and can be used to track VPS34 activity and the level of autophagy temporally and quantitatively in cells [50]. WIP1-positive puncta formation decreased significantly upon QG000052 treatment at 20 $\mu$ M relative to control conditions of amino acid withdrawal. Inhibition of puncta formation in ULK1 inhibitor treated cells mimicked results seen with the known autophagy and lipid kinase inhibitor wortmannin (**Figure 3c**).

### **3.5 Temporal initiation of autophagy and ULK1 activity and workflow**

Previous research has demonstrated that autophagy is a temporally dynamic process and the coordination between LC3 positive puncta, ATG5-12 conjugation and Beclin1 presence can occur in less than 15 min [38]. However, many studies examining ULK1 and the dynamics of autophagy often starve cells of nutrients for over 18h. Chronic starvation achieves a robust signal, but significantly lacks any physiological relevance. Therefore, prior to examining the effects of QG000052 *en masse* we performed several time course experiments to determine the

most appropriate time to inhibit ULK1 kinase activity. Supported by published temporal observations, we notice changes in autophagy as early as 15 min following complete starvation. We identified a significant change in LC3 lipidation as early as 15min (**Figure 4a**). Lipidation of LC3 can be visualized by a molecular weight shift to a lower, distinct band by Western blotting. A 30min time course was ultimately chosen as a point of known, active autophagy, but a point where negative feedback secondary mechanisms mediated by mTORC1 and AMPK phosphorylation would be less confounding relative to longer time points.

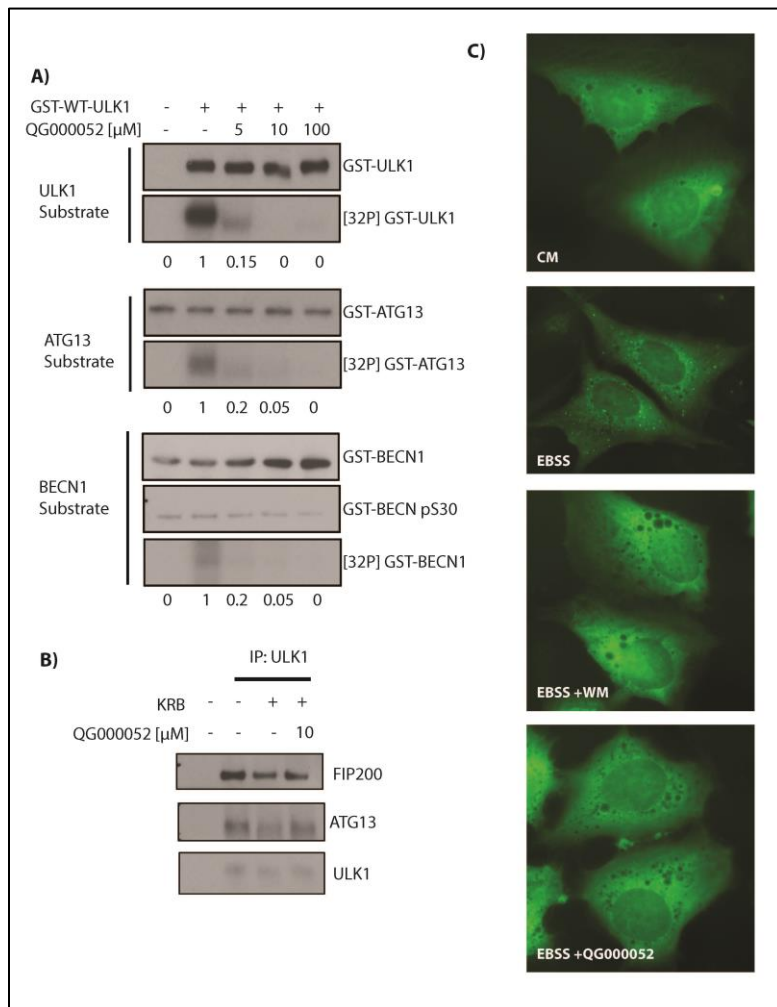


**Figure 3. QG000052 potently inhibits ULK1 autophosphorylation and kinase activity towards known substrates in vitro and in vivo**

**A)** Representative Western and  $^{32}$ P-y-ATP incorporated blots of ULK1, ATG13 and BECN1 with densitometry given below blots (n=3). **B)** ULK1 binding assays was performed with and without the presence of the ULK1 inhibitor, QG000052, under nutrient limited conditions to assess the impact of inhibition on ULK1-complex formation. **C)** GFP-WIPI1 puncta, a marker of autophagy, was assed in full media (CM) or following nutrient withdrawal in U2OS cells treated with wortmannin (WM) or the ULK1 inhibitor QG000052. Puncta formation can be clearly seen in cells starved with Earle’s Balanced Salt Solution (EBSS) alone

In order to quantitatively compare starved wild-type cells to starved cells treated with QG000052, stable isotope labelling was performed to induce a mass difference that could later be tracked through a mass spectrometry based approach [35]. Cells were grown in media containing stable-isotope labelled lysine and arginine for 3 passages, across experimental and

control conditions (**Figure 4b**). Following complete metabolic labelling, light-labelled cells were starved for 30min in KRB and given DMSO as a mock control and heavy-labelled cells were starved for 30min in KRB and supplemented with 20 $\mu$ M QG000052.

Following lysis of two biological replicates, protein concentration was determined by BCA and normalized across biological replicates and between experimental conditions. To validate the action of the ULK1 inhibitor *in vivo* and ensure metabolic labelling did not have secondary effects, we probed for pS30 Beclin1, pT172 AMPK, AMPK, ULK1, pS555 ULK1, pS755 ULK1, pS476 ULK1, pS859 Raptor, p62/Sequestrin and  $\beta$ -Actin as a loading control (**Figure 4c**). Importantly, treatment of cells with QG000052 is seen to reduce the ULK1 phosphorylation of Raptor at Serine-859, but does not significantly perturb the phosphorylation of ULK1 or AMPK. Interestingly phosphorylation of Beclin1 at serine-30 was not significantly reduced. ULK1 phosphorylation at Serine-555 is somewhat reduced, which may be explained by conformational changes brought about by the inhibitor, however other ULK1 phosphorylation sites remained unchanged following drug treatment (**Figure 4c**).

### 3.6 Quantitative results

The quantification of identified peptides was performed in the full scan of the mass spectrometer prior to the collision-induced dissociation (CID) of peptides into fragment ions to allow peptide identification. This technique readily allows for the quantification of peptides from the binary experimental conditions, as peptides share the same ionization efficiency in the gas phase, and co-elute from nano-liquid chromatography [35]. We further optimized this technique for our experiment to confidently detect a large number of peptides and allowed for the ten most abundant ion species to be dissociated following a full scan. This ‘top-10’ technique comes as a relative compromise to only selecting the three most abundant species in a scan in terms of abundance fragment ions and subsequent peptide identification, but it has been highlighted previously in phosphoproteomic screens to detect the greatest number of total proteins [45].

Due to technical issues with the Immobilized Metal Affinity Chromatography (IMAC) step to enrich for phosphopeptides, few phosphopeptides were identified as compared to similar phosphoproteomic screens. In total we identified 270 phosphorylation sites, including sites in the proteins RPLP1, XRN2, NUCKS1, SYNE1, SRRM1, PSMA3, and LRRC16A. While ULK1 inhibitor-mediated changes were identified, data collection did not produce results which could be analysed confidently to reflect the underlying biology of the system. It is likely that the SCX-

IMAC step led to subsequently poor data collection as we identified a similar number of proteins between biological replicates but were not able to identify a large number of proteins in early fractions of SCX as expected (**Figure 4d**).

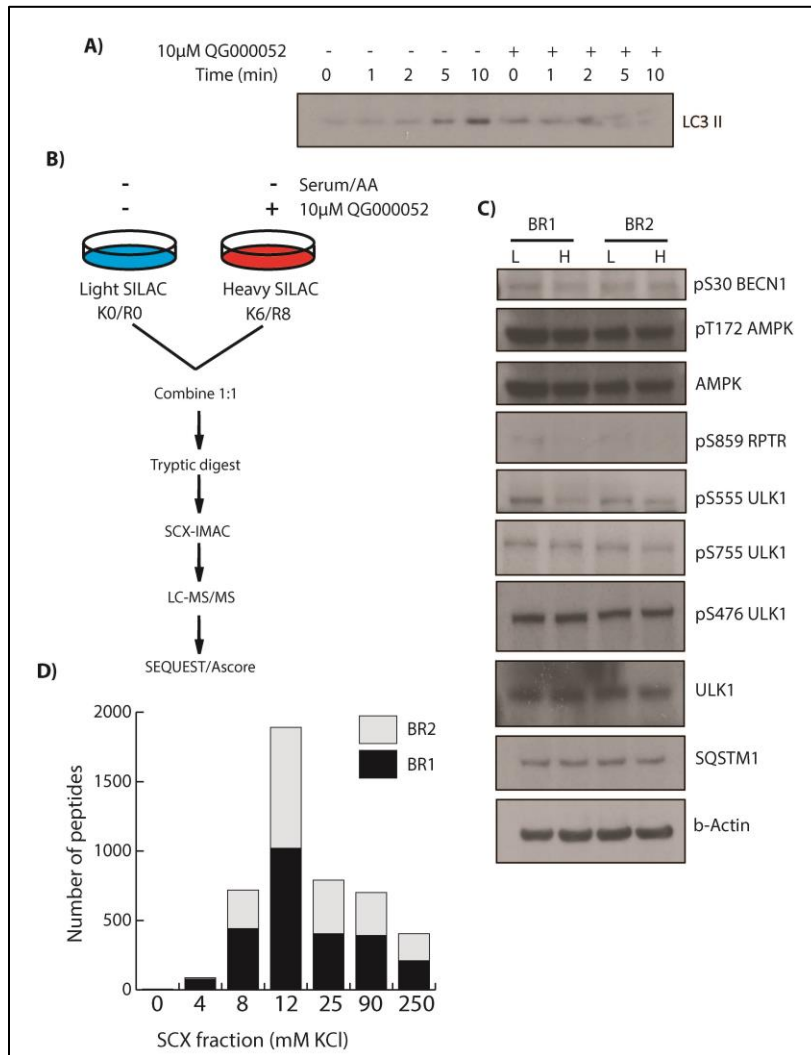


**Figure 4. SILAC-based workflow to identify ULK1-mediated phosphoproteomic changes**

**A)** HEK293 cells were starved of nutrients in KRB for each experimental time point with or without the ULK1 inhibitor. Cells were immediately lysed on ice and flash frozen in liquid nitrogen. Total LC3I/II levels were probed for by Western blot. **B)** HEK293 cells were allowed to incorporate stable-isotope labeled amino acids (either un-labeled lysine and arginine [K0/R0] or heavy labelled lysine and arginine [K6/R8]) for 4 passages prior to cell-based experimentation. Six 25cm plates were cultured to 90% confluency and starved for 30 minutes with KRB in the presence or absence of QG000052. Cells were lysed in ice-cold 8M Urea lysis buffer complete with protease and phosphatase inhibitors. Cell

lysates from inhibitor-treated and control plates was normalized by Bradford assay according to the manufacturers protocol (Piercenet), and combined at a 1:1 ratio. Reactive cysteines were reduced with DTT and alkylated with iodoacetamide prior to a tryptic digest with a trypsin to lysate ratio of 1:100. Tryptic peptides were purified from enzyme and Urea and subjected to fractionation by strong-cation exchange (SCX). Each fraction then underwent phosphopeptide enrichment via immobilized metal affinity chromatography (IMAC). Peptide and buffer impurities were removed and peptides were concentrated prior to quantitative mass spectrometry. **C)** Prior to enzymatic digestion with trypsin, the relative inhibition of ULK1 kinase activity towards known interactions and normalization of protein concentration was examined by Western blotting. **D)** Following SCX-IMAC workflow, peptides were grouped by SCX fraction

to determine the number identified in each sequential increase in KCl for each biological replicate (BR1 and BR2).

Therefore, we compared total protein level changes in response to QG000052 treatment as a proof-of-principle experiment (**Figure 5**). In total, we confidently identified 464 proteins by at least two peptides. In addition to identifying a number of housekeeper proteins such as histones, cytoskeletal proteins and chaperones, we also identified signalling proteins such as DNA-PKc and ARF1 (*Supplemental Table S4*). With a functional workflow validated, this experiment could quite easily be repeated to discover the ULK1 phosphorylation motif.

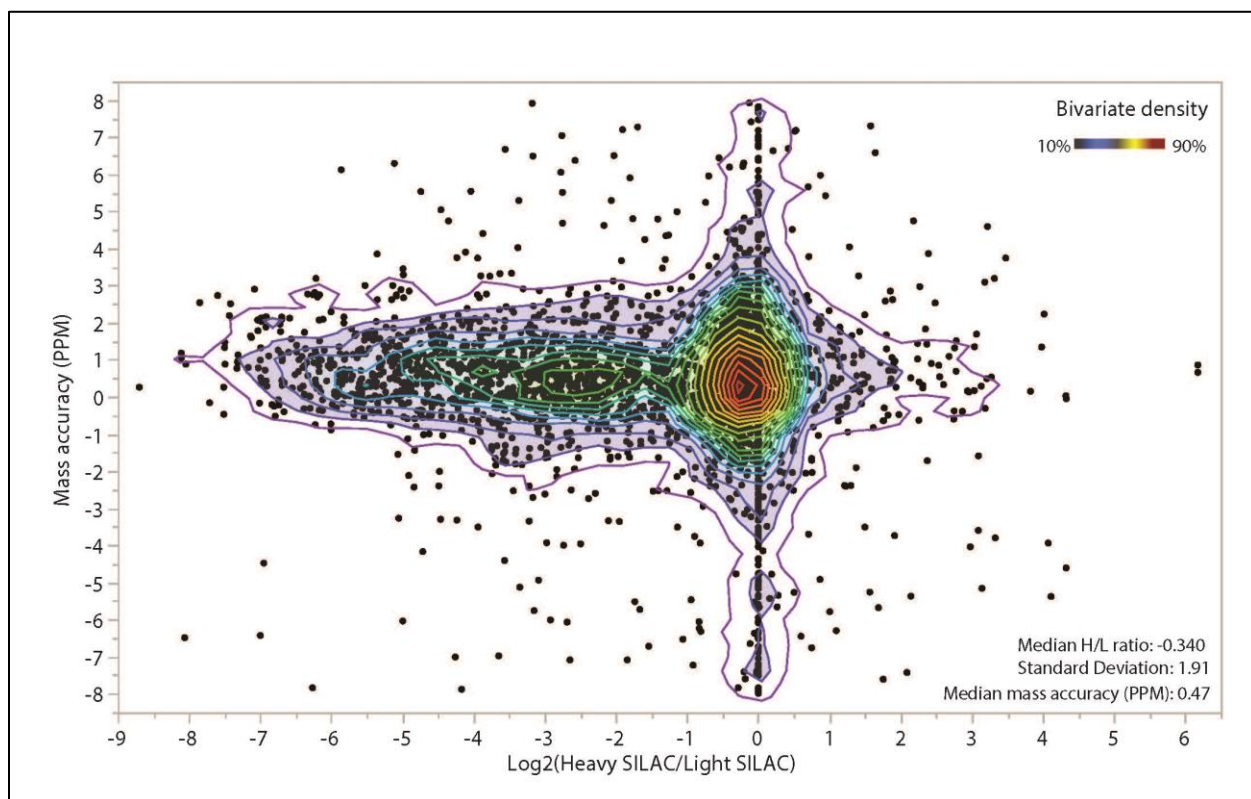


**Figure 5. Bivariate density analysis plotting the measured mass accuracy of the precursor phosphopeptide ions (in ppm) with peptide  $\text{Log}_2(\text{Treated}/\text{Untreated})$  SILAC ratios**  
All phosphopeptides from the two biological replicates were plotted based on mass accuracy of peptide identification (mass accuracy) and peptide quantification ( $\text{Log}_2(\text{QG000052-Treated}/\text{Untreated})$  ratio). Indicated are QG000052-upregulated and -downregulated peptides. The data inside of the lowest bivariate density curve represents 90% of all phosphopeptides, with minor lines corresponding to 5% density differences.

## Chapter II

### Novel biology of the tumour suppressor FLCN

#### 3.7 Identification of novel FLCN binding partners and validation *in vivo*

In addition to identifying novel ULK1 binding partners, we sought to identify binding partners to the ULK1 target, FLCN, due to its role in disease and the reported discrepancy of its function in autophagy. Further, as we identified FLCN as an ULK1 interacting protein, it became a more attractive target to elucidate. To identify new FLCN binding partners, GST-tagged human FLCN was overexpressed through transfection into HEK293 cells. Following lysis, GST-FLCN and its interacting partners were purified on glutathione-Sepharose resin and resolved by SDS-PAGE (**Figure 6a**). Gel bands were excised, proteolytically digested, and proteins were identified by mass spectrometry. We confidently identified known FLCN interacting partners such as GABARAP, FNIP1 and FNIP2, and in total identified over 100 novel FLCN interactions with high confidence based on protein coverage and number of mass spectra identified (*Supplemental Table S5*).

The list of proteins identified by mass spectrometry was subjected to bioinformatics analysis to discover gene ontology enrichments in an unbiased fashion. We used the DAVID bioinformatics program to specifically identify enriched molecular functions and protein domains found in the FLCN-interactome whose significance was determined as a function of gene ontology p-values (**Figure 7a and 7b**, *Supplemental Table S6 and S7*). Supporting recent results from other labs to suggest the role of FLCN as a modulator of autophagy and mTORC1 signalling, we identified proteins involved in translational elongation as FLCN-binding proteins. These include ribosomal proteins and EEF1A2. Moreover, FLCN may play a role in transport, as suggested by binding proteins with a HEAT domain. HEAT domains are long solenoid domains composed of alpha-helical bundles that are found in transport proteins including huntingtin (HTT) and protein phosphatase 2 (PP2a). HEAT domain-containing proteins that we identified include but are not limited to HTT, CKAP5, IMO5, HEATR1, PPP2R1A, BTAF1, and ATR (*Supplemental Table S7*).

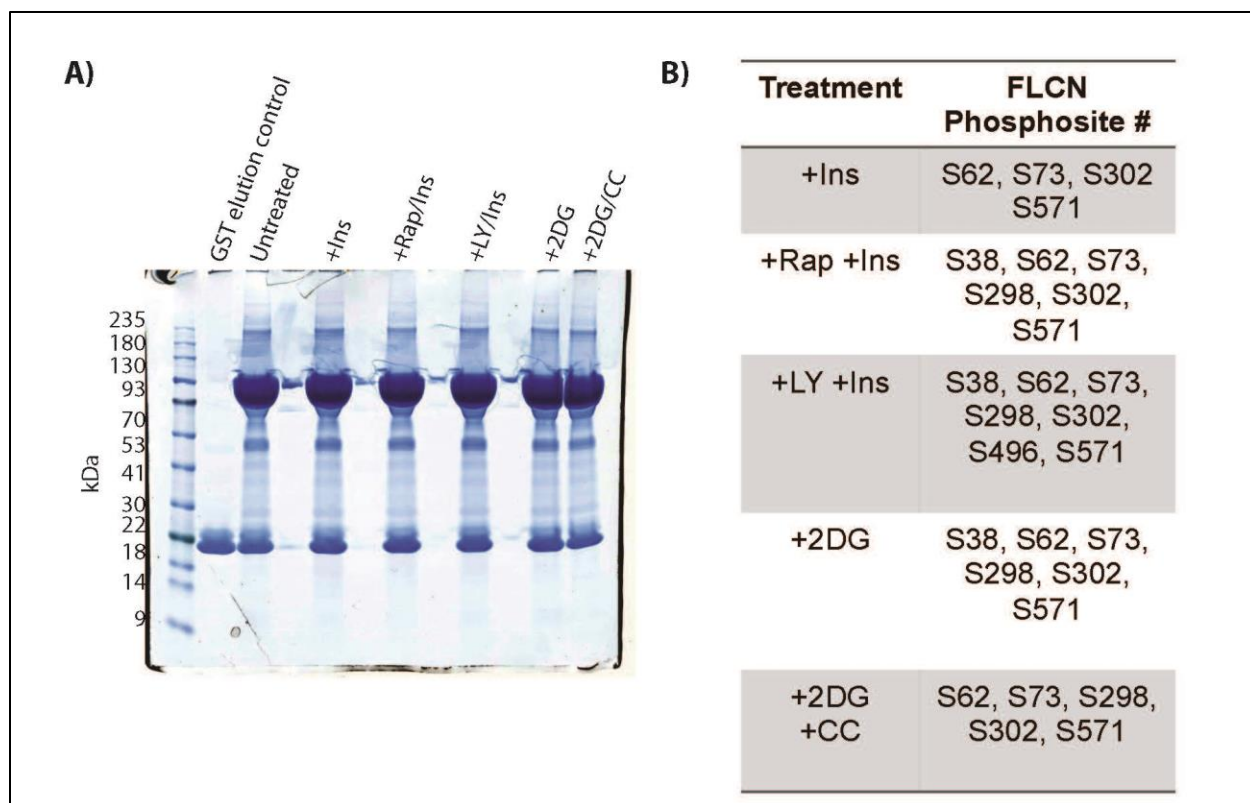


**Figure 6. FLCN is heavily phosphorylated at proline-directed serine residues)** To identify FLCN phosphorylation sites and potential kinases HEK293 cells were transfected with full length GST-FLCN and untreated, or treated with insulin (INS), Rapamycin and insulin (RAP/INS), LY and insulin (LY/INS), 2-Deoxy-glucose alone (2DG), or 2-Deoxy-glucose and compound C (2DG/CC). FLCN and its interacting partners were then GST-purified, separated by SDS-PAGE and visualized by coomassie brilliant blue staining. A total of six bands were excised from each lane, with care to isolate the large GST-FLCN band by itself. **B)** Phosphorylation sites identified and localized by LC-MS/MS for each experimental condition are provided. Site numbering follows the SwissProt-reviewed full-length protein sequence. The full mass spectrometry-based dataset for FLCN phosphorylation sites is provided in *Supplemental Table S6 and S7*.

### 3.8 Identification of FLCN phosphorylation sites and modulation by pharmacological inhibition

In order to understand possible functional roles of FLCN, cells were treated with various signalling pathway inhibitors and then FLCN phosphorylation sites were identified by mass spectrometry. HEK293 cells over-expressing GST-FLCN were left untreated or treated with insulin, insulin and rapamycin (mTORC1 inhibitor), insulin and LY294002 (PI3K inhibitor), 2-deoxyglucose (glycolysis inhibitor), or 2-deoxyglucose and Compound C (AMPK inhibitor). Gel bands corresponding to GST-FLCN were excised and digested with trypsin. In order to identify



FLCN phosphorylation sites, spectra generated by mass spectrometry were matched to either the full-length FLCN protein or its reverse sequence as a target decoy approach to reduce false peptide sequence assignments. The Sequest search algorithm, which employs a cross correlative strategy, was used to assess the number and validity of matching fragment ions from experimental against the same theoretically generated spectra. In effect, the algorithm provides a peptide sequence identity for each spectra based on a statistical framework and can be evaluated and manually validated by expert analysis. The forward and reverse amino acid sequence of the full-length FLCN protein was utilized so peptide assignments arising from the known-wrong (reverse) sequence could be used to assess the percentage of unknown-wrong assignments. Although trypsin was used as the proteolytic enzyme to generate peptides, we allowed for no specific enzyme preference in the search as a second measure of data quality. After searching data against our synthetic database, our confidence in *bona fide* phosphopeptide identification and site localization was increased to only include true hits (0%FDR) and required phosphopeptides to have an Ascore greater than or equal to a value that confers 99% site localization [37]. As a result, we confidently identified phosphorylation at serine-38, serine-62, serine-73, serine-298, serine-302, serine-496 and serine-571 of FLCN (**Figure 6b**). No threonine or tyrosine phosphorylation sites were identified using our experimental conditions, although they were allowed as variable modifications in all data searches using the SEQUEST algorithm. To understand FLCN phosphorylation in a quantitative manner, we used a chemical labelling strategy to compare untreated samples to conditions of pharmacological inhibition. To perform such a strategy, following tryptic digestion of FLCN from each experimental condition, an equal amount of peptides were labelled through a reductive amination reaction, which adds a dimethyl group to peptide N-termini and C-terminal lysine residues. Untreated FLCN was labelled with isotopically pure dimethyl groups containing  $^1\text{H}$ , while all experimental conditions were labelled to contain isotopically pure deuterium ( $^2\text{H}$ ). Labelled peptides from each condition were separately combined with labelled peptides from the untreated control condition at a ratio of 1:1 (*wt/wt*). Chemical labelling allowed for peptides to be quantified based the induced mass difference so distinct *m/z* states could be resolved by mass spectrometry and not effect peptide elution from liquid chromatography as  $^2\text{H}$  and  $^1\text{H}$  species share the same structure. We were able to readily identify and quantify phosphorylated FLCN with this workflow, yet large standard deviations did not permit any great biological elucidation even following a normalization to the



non-phosphorylated, quantified FLCN peptides (*Supplemental Figure S2, Supplemental Table S8*).

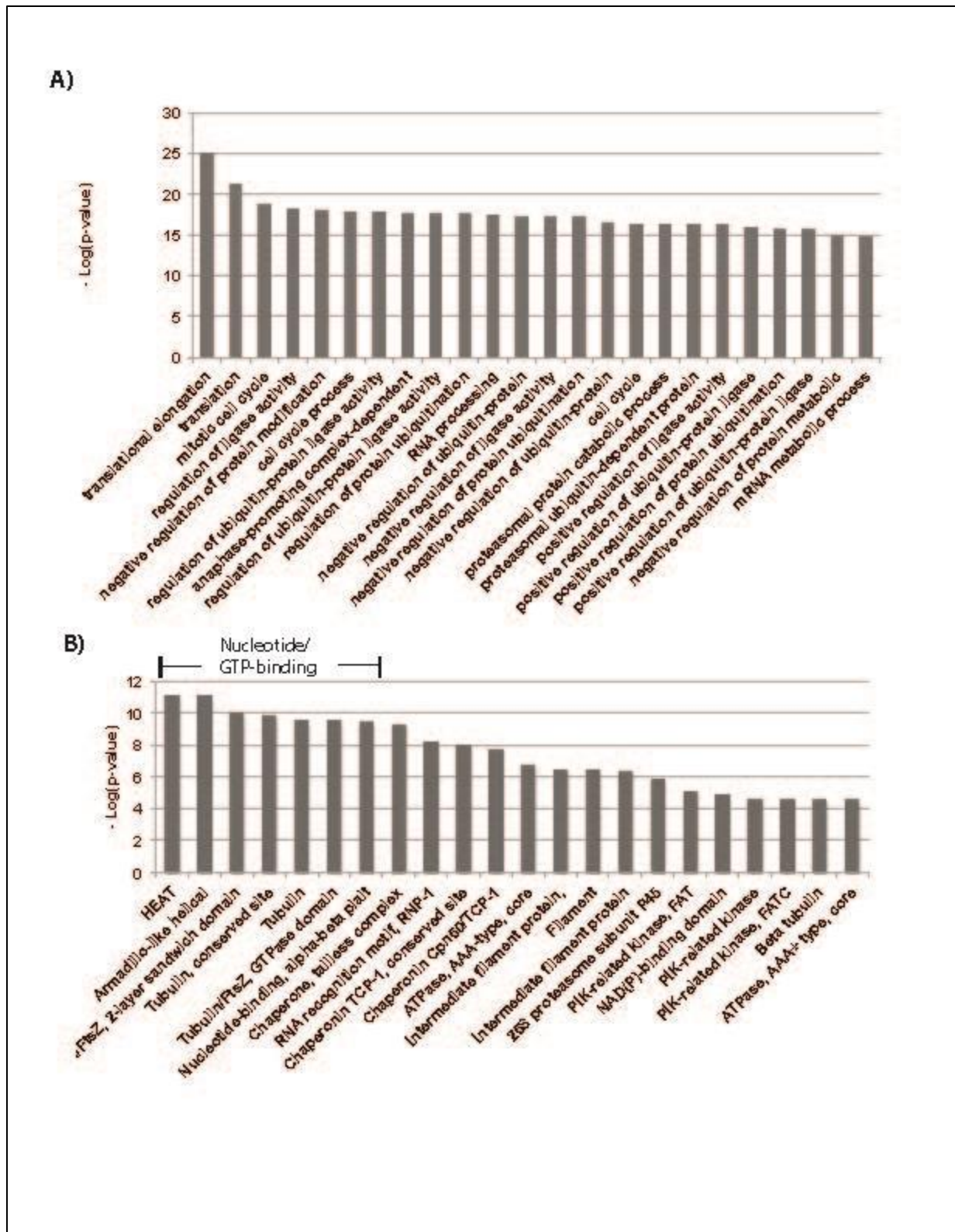


**Figure 7. Gene Ontology enrichment identifies FLCN to have roles in transport and translation** A) Enriched biological processes are given as a function of p-value generated by uploading the full list of FLCN binding proteins to the DAVID bioinformatics portal in the IPI

format (<http://david.abcc.ncifcrf.gov/>). The top twenty-four GO biological process terms are provided. The full gene list for each term can be found in *Supplemental Table S4*. B) Enriched functional protein domains from FLCN binding partners were identified using the DAVID bioinformatics portal and INTERPRO domain annotation. The top twenty-two identifications are provided and the full list of gene names can be found in *Supplemental Table S5*.

Of the phosphorylation sites identified, serine-38, serine-62 and serine-571 were found to the greatest extent and to the greatest stoichiometry across conditions in both quantitative and binary analyses (*Supplemental Table S2, S3*). Interestingly, LY294002 treatment induced phosphorylation at serine-496 which was not identified under other conditions, suggesting the possibility of PI3K-regulated changes in FLCN modification. Although this remains a binary comparison, outside of this site pharmacological inhibition by other drugs did not produce significant changes in phosphorylated amino acids. This comes as a surprise as previous work has identified the TSC2-mTOR pathway to regulate FLCN phosphorylation at serine-62 and serine-302 in HeLa, HEK293 and Cos2 cells through over-expression studies [26]. While robust changes in FLCN phosphorylation—as detected by site-specific antibodies and inferred through mobility shift upon protein separation by SDS-PAGE—were seen, the results could not be recapitulated in our hands under a more advanced proteomic approach. It is possible to mitigate disparate findings by comparing the concentration of inhibitor used; however, a more likely interpretation is that multiple kinases phosphorylate FLCN, and over-expression or robust depletion of specific kinases is required.

The majority of FLCN phosphorylation sites were found to be proline-directed; phosphorylated serine residues in FLCN are followed at the +1 position by a proline residue. While not entirely reductive, this finding rules out the specificity of several kinases and kinase families. Indeed from structural studies, we know that basophilic kinases, such as PKA, PKG and PKC (AGC kinases), calmodulin-dependent protein kinases (CAMK kinases) and the majority of serine/threonine kinases and phosphatases heavily disfavour proline at the P+1 position [51, 52]. On the other hand, cyclin-dependent protein kinases (CDKs) and mitogen-activated protein kinases (MAPKs) are both proline-directed, which suggests FLCN may be induced by cell-cycle dependent mechanisms. Indeed CDK2 was identified in our screen and other kinases such as polo-like kinases and aurora kinases are likely modifiers of FLCN. This hypothesis is supported by the identification of aurora kinase A (AURKA) in our proteomic screen, and the fact that polo-like domains readily bind pS-P-X motifs (*Supplemental Table S5*) [53]. Interestingly, all of

the kinases suggested thus far regulate some aspect of commitment to cell cycle or its subsequent regulation.

To analyse the phosphorylation state of FLCN and its known, functional complex further, we performed assays to enrich for FNIP1, FNIP2 and a regulator of mTORC1 signalling, TIP41. We identified 5 novel phosphorylation sites on FNIP1, 8 novel phosphorylation sites of FNIP2 and 3 novel phosphorylation sites on TIP41 (*Supplemental Figure S4*). To study FNIP1 phosphorylation we co-transfected either full-length ULK1 or ULK1<sup>K48I</sup>. We identified 9 total phosphorylation sites on FNIP1 and just over half of the sites identified were found upon co-transfection with wild-type ULK1. In terms of phosphorylation site location on FNIP1, the sites identified are found throughout the full length of the relatively large protein and interacting domain with FLCN. With regards to FNIP2, we identified a total of 15 phosphorylation sites by either transfecting cells with FNIP2 alone, or co-transfecting with ULK1. Interestingly, more FNIP2 phosphorylation sites were identified without co-transfection of ULK1. All sites identified by co-transfection with ULK1 were also identified in FNIP2 alone, suggesting that ULK1 does not phosphorylate FNIP2, or, overexpression of ULK1 actually negatively regulates FNIP2 phosphorylation. We also identified phosphorylation sites in the AMPK-binding domain of FNIP2. TIP41 phosphorylation, a regulator of the PP2a phosphatase, and subsequent regulator of mTORC1 signalling, was also examined by incubating cells with insulin alone, or with insulin and rapamycin. Only three phosphorylation sites were identified on TIP41, however, none of these sites have been annotated in either Uniprot or the Phosphosite repositories for post-translational modification data. One unique phosphorylation site on TIP41 was found in each experimental condition (*Supplemental Table S10, Supplemental Figure 4*).

### **3.9 FLCN-interactome related to disease progression and common disease phenotypes**

The list of FLCN binding partners was manually interrogated to examine possible interactions, which may play a role in the disease progression of BHD, or, already have a known pathological function. We wanted to determine if these potential FLCN interactions could be validated. Therefore, we employed an immuno-affinity enrichment endogenous FLCN from HEK293 cells, and blotted with antibodies against several identified proteins including SUZ12, TAB1, TAK1, ULK1, CAD, mTOR and FASN (Figure 8). Several proteins, including FASN and CAD, although identified by mass spectrometry with a high number of spectra are possible

contaminating proteins, and GST binding alone could not be ruled out. Therefore, outside of SUZ12, data from endogenous immunoprecipitations is omitted for this manuscript.

While CAD may in fact be a contaminant, as many repeated attempts to validate its endogenous interaction with FLCN by pull-down have yielded few positive results, its validation as a FLCN binding partner holds much promise and much interest from previous work in the field. Through personal communication a collaborator, Lisa Henske (Harvard Medical School, Boston), evidence from lower organisms is mounting to support a *bona fide* interaction between FLCN and CAD. CAD is essential for *de novo* pyrimidine biosynthesis and acts as a fusion of four catalytic activities, underlying the rate limiting steps of the anabolic process, and further, its activity is regulated by mTORC1 signalling and is directly phosphorylated at serine-1859 by S6K1. This phosphorylation event specifically enhances the E3 activity of CAD *in vivo* to synthesize new pyrimidine nucleotides [54]. Further, CAD has also been identified as a binding partner of Rheb, the small G protein that inhibits mTOR, in a GTP-dependent manner. GTP-Rheb over-expression localizes CAD to lysosomes, suggesting a role for pyrimidine biosynthesis or inhibition through localization. The implication of Rheb involvement and its true validation as a binding partner remains somewhat myopic as all studies were performed by over-expression [55]. Our identification of mTOR by mass spectrometry (yet to be validated endogenously) complicates this story even further (*Supplemental Table S5*).

It is equally exciting, paradoxical, and mechanistically frustrating that FLCN is found throughout mTOR related signalling pathways yet we cannot readily say where in the pathway it functions. If FLCN truly binds CAD—as it does so many other proteins—it should be hypothesized that FLCN may play a greater role in localization and complex formation rather than any one unique catalytic activity. Indeed, due to the discovery of so many interacting proteins, we may want to compare similarities between several functionally distinct FLCN targets in parallel to gain insight into its function. The most readily accessible way to direct this comparison would *not* be based on crystallographic or *a priori* structural knowledge alone. Already the list of validated FLCN targets suggests many distinct binding modalities, some of which are likely facilitated by FNIP1 and FNIP2. Further, we know from structural and sequence information that distinct protein:protein interactions rarely if ever occur through competition for exactly the same amino acid sequence. Therefore perhaps the best way to assess the molecular function of FLCN is by comparing its interaction with a single type of enzyme in two distinct,

well-established signalling pathways. With this assertion, the serine/threonine protein kinase TAK1 (MAP3K7), which plays a role in innate immune signalling through TRAF6—also an ULK1 modifying E3 ubiquitin ligase—and TGF-beta signalling, could readily be compared to another kinase identified in our screen, Aurora Kinase A (AURKA). Examining the same class of enzyme streamlines to a shared functional readout so comparisons can be drawn by kinase assay. Further as AURKA functions in the nucleus and TAK1 has no acknowledged nuclear function, these targets could be used to examine how FLCN mutational status dictates protein localization and function [56].

### **3.10 FLCN as a regulator of biology in the nucleus and primary cilia**

Of further interest and intellectual complexity, SUZ12, a key component of the polycomb repressive complex, which silences gene expression through histone methylation, was validated as an endogenous interacting partner of FLCN (**Figure 8a**). Loss of the polycomb repressive complex including SUZ12 has been shown to amplify RAS signalling in cancer [57]. Furthermore, SUZ12 mutation has been found as a common mutation in peripheral nerve sheath tumours in a related tumour syndrome, neurofibromatosis type 1 (NF1) [58, 59]. Outside of our novel finding of SUZ12 direct binding to FLCN, no data has connected SUZ12 to BHD Syndrome and the molecular consequence of this interaction remains unknown, although it is likely to affect cell differentiation as *Suz12*<sup>-/-</sup> embryonic stem cells are unable to undergo proper differentiation [60]. With regard to transcriptional regulation and genome integrity, we further identified DNA-PKc, a kinase that acts as a sensor for DNA damage, as a FLCN binding partner (**Figure 8b**). These endogenous validations open a completely novel avenue of BHD and FLCN-related research towards understanding genomic anomalies propagated in the disease state.

Somewhat distinct from its acknowledged proclivity for neoplastic induction, BHD has recently been shown to act as a ciliopathy; a disease propagated by dysfunctional primary cilia. We wanted to further understand and examine cilia signalling components by assessing temporally-dependent changes following gene knockdown [34]. Upon a close inspection of our proteomic investigation, we identified a significant number of cilia-specific or cilia-related protein components. For example, FLCN was found to bind components of the CCT/TRiC family of chaperones which mediate BBSome assembly and primary cilia formation [61]. FLCN was also found to bind Aurora kinase A (AURKA) which regulates primary cilia stability

through the phosphoinositide signalling of inositol polyphosphate 5-phosphatase E (INPP5E), and further, disassembly through a calmodulin-dependent mechanism (*Supplemental Table S5*) [62, 63]. Additionally, we identified a number of proteasomal proteins as FLCN binding partners, which is particularly exciting, as recent evidence has demonstrated an essential role for the proteasome in the formation and extension of the primary cilia axoneme. Significant cross-talk between the primary cilia, the proteasome and autophagy—all biological realms that FLCN has been suspected to act upon—are areas which require further attention for a better understanding of ciliopathies [64-66].

FLCN was also identified to bind a number of components of the nucleopore complex, yet few of these proteins have been identified to localize to the primary cilia transition zone, a secondary site of nucleopore protein action [67]. The identification of NUP50, NUP53, NUP54, NUP133, NUP150, NUP153, NUP155, NUP160, NUP188 and NUP205 suggests that FLCN has some largely unknown role at the nucleopore (*Supplemental Table S3*). Since FLCN has been shown to act on the small G-protein complex Rag-C/D to participate in mTOR signaling, it is not unlikely that FLCN could bind and regulate additional small G proteins such as Ran, a critical mediator of trafficking to the nucleus and primary cilia. This binding event could regulate FLCN to a greater extent than Ran, and dictate the localization and binding capacity of FLCN as well. With supporting evidence from our lab and others, it is hypothesized that FLCN may provide a Ran-directed trafficking function through direct binding and post-translational modification status. Indeed, FLCN shares some homology to DENN domain containing proteins which regulate Rab small GTPases. However FLCN likely employs a slightly different mechanism as it is missing the conserved consensus FCFP motif in uDENN domains and widely conserved SxLxPxFxxxxxxL motif in DENN domains (*Supplemental Figure S3*) [68].

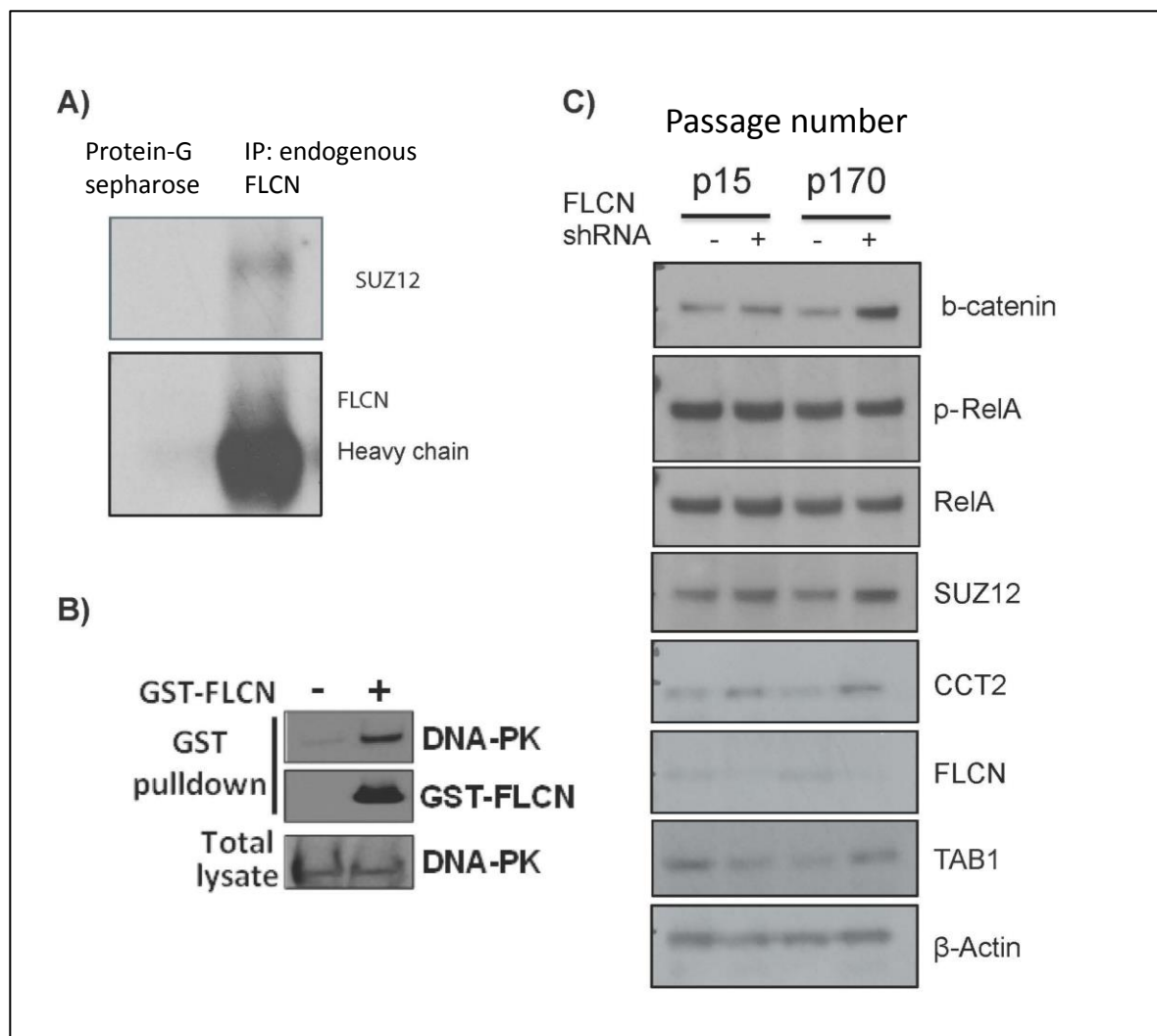


**Figure 8. Validation of novel endogenous FLCN interactions and relationship to Birt Hogg Dubé Syndrome disease progression**

**A)** FLCN was purified by immunoprecipitation and controlled for by incubating lysate with protein-G sepharose in the absence of anti-FLCN primary antibody. FLCN binding proteins were probed for with antibodies against SUZ12 and DNA-PKc. **B)** GST-FLCN was expressed in HEK293 cells and GST purified to identify co-immunoprecipitating proteins. DNA-pkc was probed for by Western blot in cells with or without GST-FLCN. Total DNA-pkc levels from whole cell lysate are shown as a control. **C)** UOK257 cells were infected with lentivirus containing shRNA against FLCN. Cells were passaged for 15 times or 170 times and compared to young progenitor cells. FLCN interacting proteins and proteins involved in signalling at the cilia were probed for by Western blot.

With further regard to FLCN as the etiological agent of BHD, it was hypothesized that interacting partners and key pathways activating transcription, such as the NF-κB signalling



pathway, may demonstrate protein level changes that correspond to disease progression. The NF- $\kappa$ B signalling pathway was chosen for closer examination for several reasons. First, gene-expression studies in embryonic stem cell and patient derived UOK257 cell-lines, with known FLCN mutations, showed a down-regulation of signalling components which are transcriptionally regulated by NF- $\kappa$ B, including TGF $\beta$ -RII [69]. Secondly, proteasomal function—a requirement for NF- $\kappa$ B signalling whose p105 precursor is processed to a smaller active p50 protein (NF- $\kappa$ B<sup>p50</sup>) by the 26S proteasome—was shown to be significantly dysregulated in a related ciliopathy, Bardet-Beidl Syndrome (BBS). Specifically in Bardet-Beidl Syndrome, the physical binding of the mutant etiological agents—the BBS family of proteins—to core proteasome subunits impaired proteasomal function in the disease state [65, 70]. Lastly, NF- $\kappa$ B signalling is constitutively activated in a number of cancers including renal cell carcinoma [71, 72]. Exploiting proteasomal dysregulation could be favourable in a therapeutic setting in combination with mTORC1 inhibitors as previous work suggests that alterations to proteasome function are a central characteristic of ciliopathies. Therefore, to resolve the function of NF- $\kappa$ B in BHD, work comparing the levels of the proteasomally processed NF- $\kappa$ B product, p105/p50, and other signalling proteins in tissues affected by BHD, or, in a model of BHD disease progression is critical to determine if known ciliopathies truly share this mechanistic commonality.

Without access to human tissue, we began assessing the NF- $\kappa$ B pathway and proteasome function in a model developed in human cortical renal tubule cells to recapitulate disease progression. We utilized cells at passage 15 and passage 170, with a stable, lentiviral knockdown of FLCN as “new” and “old” cells, respectively, and we began our investigation by western blotting for the protein p65/RelA, a central component of the NF- $\kappa$ B pathway. Canonically, RelA forms a dimer with NF- $\kappa$ B<sup>p50</sup> following proteasomal processing of p105 and several phosphorylation events [70]. To act as a transcription-activating complex, RelA-p50 requires stable disassociation from an inhibitory protein, Inhibitor of kappa-B (I $\kappa$ B $\alpha$ ). The inhibitory protein, I $\kappa$ B $\alpha$ , masks the nuclear localization signal of NF- $\kappa$ B and sequesters the inactive transcription factor in the cytoplasm. The RelA-p50 complex is released from inhibition by the I $\kappa$ B kinase complex, IKK, composed of  $\alpha$  and  $\beta$  catalytic subunits and a regulatory  $\gamma$  subunit. Phosphorylation of I $\kappa$ B $\alpha$  at serine-32 and serine-36 leads to dissociation and proteasomal

degradation of I $\kappa$ B $\alpha$ , allowing the active RelA-p50 dimer can enter the nucleus and function as a transcriptional activator [73, 74].

By immunoblotting for RelA, we identified no significant change in its phosphorylation at serine-536 nor protein level abundance, relative to a tubulin control, and conclude that RelA status alone is not affected by loss of FLCN. However, we detected small but significant protein level changes in IKK $\alpha$ , the core catalytic component of the heterotrimeric I $\kappa$ B complex (**Figure 8C**). IKK $\alpha$  appears to be upregulated in late-passaged, FLCN depleted cells, relative to lower-passaged cells with and without FLCN expression. This comes as somewhat of a surprise as upstream IKK $\alpha$  would likely affect the protein levels and phosphorylation status of RelA. However, a further analysis of I $\kappa$ B $\alpha$  and NF- $\kappa$ B<sup>p50</sup> levels and phosphorylation status is required to conclusively determine how the NF- $\kappa$ B may be dysregulated in BHD. Additionally, treatment with Velcade/bortezomib (PS-341), a potent inhibitor of the 26S proteasome, could be useful as a tool to understanding this pathway.

To examine possible alterations in transcription as a function of FLCN status, we used luciferase assays to experimentally determine the output of NF- $\kappa$ B signalling and TGF-beta signalling. HK2 cells depleted of endogenous FLCN were transfected transiently with pcDNA3 or cDNA to HA-FLCN, HA-FLCN<sup>K508R</sup>, HA-FLCN<sup>Y463X</sup>, or HA-FLCN<sup>H42G</sup>. Mutant variants of FLCN were chosen as they are seen in cases of clear cell renal cell carcinoma (CCRCC) or are known to significantly abrogate signalling through FLCN [75]. We hypothesized that mutations in FLCN leading to loss of function would have a significant effect on the transcription of TGF-beta or NF- $\kappa$ B regulated genes. To assess the role of FLCN on NF- $\kappa$ B and TGF-beta signalling, we co-transfected HK2 cells with luciferase reporter constructs to either NF- $\kappa$ B or SMAD, controlled for by renilla-luciferase. The SBE4-reporter construct, containing four SMAD response elements was used to examine TGF- $\beta$  signalling and a separate NF- $\kappa$ B construct was used as a distinct readout. Following transfection, cells were provided fresh media and the NF- $\kappa$ B pathway was induced through the addition of TGF- $\beta$  to a final concentration of 100ng/mL. The induction of this pathway was controlled for experimentally by treating half of the renilla-controlled and NF- $\kappa$ B reporter transfected cells with ddH<sub>2</sub>O. To assess reporter intensity in a quantitative, statistically controlled manner, each experimental and control condition was repeated in triplicate (*Supplemental Figure S2*). In addition to HA-tagged FLCN constructs, we

attempted to use GFP-FLCN<sup>S62A</sup>, GFP-FLCN<sup>S62D</sup>, and GFP-FLCN<sup>S62E</sup> constructs (data not shown).

We next sought to determine if we could identify signalling proteins with known roles at primary cilia to further support BHD as a true ciliopathy. Interestingly, Birt-Hogg-Dubé syndrome's role as a ciliopathy also ties into its known metabolic abnormalities. Cellular machinery involved in ciliogenesis participates in autophagy and blocking autophagy enhances primary cilia growth and associated signalling [76]. We examined the  $\beta$ -catenin protein as the Wnt and  $\beta$ -catenin signalling pathway is regulated by cilia. While the exact mechanism remains incomplete, it appears that functional cilia negatively regulate  $\beta$ -catenin levels. Indeed, in Bardet-Biedl syndrome, there is an accumulation of  $\beta$ -catenin as a result of deficient cilia [77]. To support the role of FLCN loss in promoting changes in cilia, we identified a significant increase in  $\beta$ -catenin levels in late passaged cells (**Figure 8c**). This suggests a significant dysregulation in cilia, similar to that seen in BBS. Further, this finding supports the previous finding that identified activation of canonical WNT signalling following FLCN knockdown [34]. Constitutive activation of WNT signalling upon FLCN loss would ultimately promote developmentally regulated transcriptional programs and progression to a neoplastic state. Additional work is needed to characterize Hedgehog signalling in BHD and FLCN-null cells, as it remains the most well characterized pathway linking primary cilia to developmentally regulated processes [78-80]. Hedgehog signalling dysregulation has been identified in related ciliopathies, but remains a point of novelty in BHD.

Outside of the primary cilium, we also examined protein level changes in the FLCN binding partner and chromatin remodelling protein, SUZ12. Of interest, SUZ12 levels increased upon the sustained loss of FLCN (**Figure 8c**). Due to the fact that SUZ12 acts as a transcriptional regulator, SUZ12 may act as a tumour suppressor to selectively repress particular genes, or, its accumulation could help further the transformation of FLCN-deficient cells. The genomic instability propagated by FLCN loss may be directly tied to chromatin remodelling proteins like SUZ12 and requires further study. Ideally, by looking at transcription-level data, or by inducing a secondary deficiency in SUZ12, we can further determine the effect this result has on disease progression and cellular transformation.

#### 4. Discussion

Here we identified novel protein interactions of the protein kinase, ULK1, and the metabolic tumour suppressor, FLCN. With regards to ULK1 many of these newly identified interactions suggest ULK1 to play a broader role outside of its known canonical contribution to autophagy. Indeed, ULK1 binding to another serine/threonine kinase, RSK4, suggests that ULK1 is able to mediate effects on other signalling pathways, or amplify its actions through further kinase recruitment. Additionally, integrating kinase signalling with vesicle formation dynamics remains a point of critical interest for further study. What signals are critically required for the formation and maturity of an autophagosome? And, how many signals are needed for short temporal responses in an energy-limited state? As studying these types of interactions are critical as novel findings in their own right, probing the functional role of ULK1 binding to targets with known roles in vesicle trafficking and formation, such as PIKfyve, will be essential to understand how the kinase dictates the autophagic status of the cell directly. Does ULK1 phosphorylate PIKfyve or the PIKfyve complex directly to alter phospholipid production, analogous to its role in Beclin1 and VPS34 complex regulation? Furthermore, does ULK1 regulation of PIKfyve act as a feedback mechanism to reduce PtdIns(3)P levels and stop autophagy? And, does the creation of PIKfyve products recruit a functionally distinct set of proteins to act at the nascent autophagosome? As a future direction, we will need to determine if ULK1 can directly phosphorylate PIKfyve, and if true, whether this modification alters the lipid kinase activity of PIKfyve. Further, now that we have established a phosphoproteomic workflow for identifying ULK1 substrates, continuing to employ this established protocol to identify more phosphorylation sites could identify PIKfyve as a regulated target.

Outside of the canonical autophagy interacting network proposed by Chris Behrends and colleagues in 2010, we also identified a connection between ULK1 and ciliogenesis. Our discovery of an ULK1 interaction with ASAP1, and identification of endosomal proteins, warrants further experimental validation and insight as energy state, cell growth, autophagy and cell cycle progression are all linked to primary cilia [76]. The direct control of initiating events in ciliogenesis by a proposed ULK1-mediated mechanism could offer additional mechanistic explanation for cellular quiescence brought about under autophagic conditions. ULK1 phosphorylation of ASAP1 could result in changes in Arf nucleotide binding and vesicle formation. Indeed, using the ULK1-inhibitor QG000052, which we were the first to validate as a

potent ULK1 kinase inhibitor over a very short time course, will be useful for understanding this mechanism. Because ciliogenesis and cilia extension and retraction is highly dynamic, a potent inhibitor like the one validated here could be used for live cell imaging of cilia where traditional genetic approaches would fall short.

To further understand ULK1-interacting partners and whether they truly participate in autophagy, RNAi experiments to knock down binding partners should be carried out. The hope in doing this experiment would be to phenocopy the results that arise from inhibition of ULK1 in cells, or, some aspect of the autophagic process. It is highly unlikely that depletion of ASAP1, for example, would exactly replicate ULK1 loss; however, if they are true binding partners some functional arm of this axis will be lost.

A finding from this study that warrants additional attention comes from our comparison of yeast Atg1 phosphorylation sites to their human counterparts. Under this analysis we begin to understand how a conserved pathway or functional system may evolve to support critical functions. Comparing the kinase-substrate library and targets of atg1 to human orthologues provides a somewhat contrary and distorted view on how autophagic machinery is canonically viewed. Although functional orthologues are widely noted, few identified phosphorylation sites share a high degree of identity. Indeed, due to this discovery that exceedingly few sites identified in this study are evolutionarily conserved, we must consider that higher metazoan autophagy—or at least processes directed by ULK1—may have evolved distinct roles to support an immune system and the period of starvation immediately following birth. While the autophagy-interactome may be similar in total, its actual dynamics may be quite different as dictated by post-translational modifications. Indeed, we would expect multicellular organisms to employ autophagic machinery in a distinct manner to unicellular eukaryotes, such as *S. cerevisiae*, as time spent in a fasting state is vastly increased and requires higher-level input and hormonal cues. Therefore, while it is entirely appropriate to suggest evolutionarily conserved protein elements in the autophagy interaction network, it is incongruous to extrapolate post-translational modification data generated in lower organisms to imply direct orthologous function and mechanism in humans. Requirements dictated through evolutionary pressure and time have likely created numerous distinct roles to support multicellular life and tissue-specific functions are confounded in the existing complexity of macroautophagy. The evolved complexity in macroautophagy, and other signalling systems, should be thought of under the lens of a model of

best fit, in which existing proteins are repurposed or given expanded function through changes in their degrees of freedom to subsequently the interaction network. An interesting preliminary investigation into this line of inquiry could be to consider potential differences arising from a quantitative phosphoproteomic screen against the same conserved kinase in different model organisms with a highly potent and selective inhibitor. This could answer if the same quantitative and site-specific differences arise across evolution, and, how conserved the autophagy-specific phosphoproteome is across species. While this study would be a fairly major undertaking it would elucidate sub-networks which arise as a consequence of evolution in a specific biological process.

If we take a step back and consider ULK family kinase function alone, it appears to have necessary intrinsic, exogenous stress-induced actions similar to innate immune signalling whereby function—while pleiotropic—is only realized upon physiological barriers. Put simply, it is only through barriers and stressors to homeostasis do we likely realize some functionality. While ULK1 and ULK2 knockout studies have established a functional significance of autophagy in development, a second question remains: would endogenous over-expression of ULK1 or ULK2 result in altered primary metabolism, increased neoplastic potential, or altered immune functions?

With regards to the tumour suppressor FLCN, we discovered a number of proteins and biological processes which the metabolic tumour suppressor is likely to regulate through direct interaction. Through bioinformatics, we also identified proteins domains in FLCN binding proteins which suggest further functional roles. The greatest up-regulated biological processes and domains were translation, cell cycle, regulation of protein ubiquitination, as well as HEAT and nucleotide binding domains. While the exact mechanism of many of these interactions remains somewhat nebulous, the identification of a number of proteins in mTORC1 signalling further solidifies its role as a metabolic tumour suppressor and regulator of this signalling pathway. Due to the fact that endogenous purification of FLCN and interacting proteins has remained a difficult task, using over-expression studies to validate some of these interactions will prove crucial. Moreover, as we identified protein level changes in some FLCN interactions, it would be interesting to extend this finding and probe for mTORC1 signalling components. Is the stoichiometry or localization of mTORC1 components significantly altered or directly influenced by FLCN loss?

By confirming direct interaction with several proteins that regulate transcription and genomic integrity, SUZ12 and DNA-PKc, we found further future directions to study FLCN as the etiological agent in Birt-Hogg-Dubé syndrome. These identifications support the acknowledged role of FLCN as a metabolic tumour suppressor involved in DNA damage repair; yet, they also put forth more nuanced roles for the protein with both cytoplasmic and nuclear functions. While not covered in this study, work from our lab has built upon these original interactions to demonstrate that functional loss of FLCN significantly affects genomic integrity as measured by an assay to detect telomere length as well as increased accumulation of DNA damage as FLCN-deficient cells are grown in continuous culture (as observed by  $\gamma$ -Histone 2AX phosphorylation). Knockdown of FLCN recapitulated our hypothesis and supported interactions. To further support this work we identified that several FLCN binding proteins change in a cell culture based model of BHD syndrome over time. Oddly, a number of FLCN binding protein accumulate systemically in response to FLCN loss which underlying various discrete signalling systems. Supporting previous work from other labs, we found that primary cilia proteins appear to be dysregulated and  $\beta$ -catenin is significantly up-regulated in old HK2 cells depleted of FLCN relative to lower passage counterparts.

It is yet to be determined if BHD is truly similar to other ciliopathies with regards to altered proteasomal function, however the accumulation of these proteins is fairly suggestive. Further work will need to be done to determine if BHD functions in a manner similar to Bardet-Beidl syndrome, where proteasomal function is blunted, and to determine which specific cilia receptors and signalling pathways are down-regulated by loss of FLCN. Support for this mechanism will provide additional therapeutic opportunities for treating BHD, as proteasomal inhibitors can be tested in preclinical models.

Although we identified protein level changes in FLCN binding proteins to support and expand the classification of the syndrome as a ciliopathy, we also found changes that highlight significant, novel avenues of research. Indeed, the identification of a number of nucleopore proteins supports a role of FLCN in protein trafficking into the nucleus. We identified the NUP50, NUP53, NUP54, NUP133, NUP150, NUP153, NUP155, NUP160, NUP188 and NUP205 as binding partners of FLCN. These proteins are found at different areas in the nucleopore complex architecture, and some are located at the cytoplasmic, core, and nuclear sides of the complex. This proteomic finding, along with bioinformatics evidence suggests that

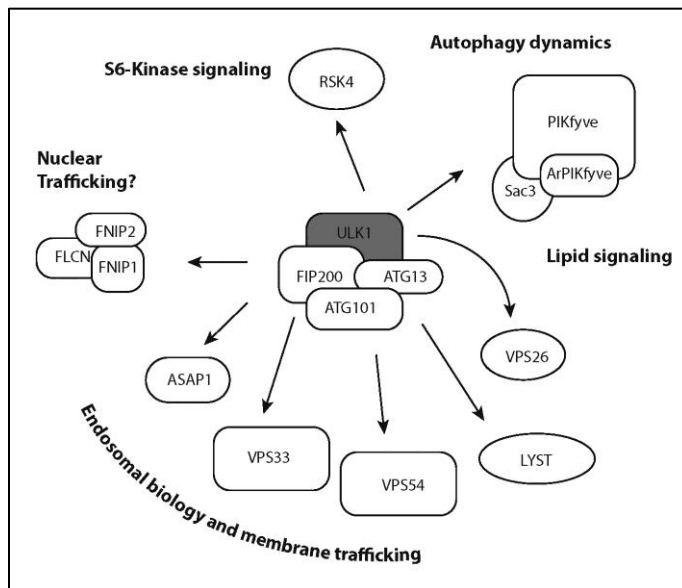
FLCN is highly tied to the nucleopore and likely has some trafficking function which is yet to be resolved. Current work by our lab and others suggests temporal localization and direct binding of FLCN with the nucleopore complex, and continued research to investigate this functional interaction will explain how FLCN and its loss may affect nuclear biology. More work needs to be done to assess which nucleopore proteins, and at what affinity FLCN is seen to be a binding direct partner. This will require further biochemical or *in vitro* approaches and pull-down strategies. Additionally, biophysical approaches like Biacore reaction could be used here.

Overall, further interrogation of our proteomic datasets and their integration with this model of disease progression will be critical to understanding how loss of FLCN can lead to renal cancer development. It will be interesting to see if any interactions could potentiate novel treatment options, or, the repurposing of existing treatments for BHD and related ciliopathies. As we come to understand this set of rare diseases to a greater extent there is a significant hope to find commonalties to exploit. Indeed with this being said, a continuation of research into FLCN biology could go any number of directions. The most logical future progression of this research would be to determine if proteasome function is altered and if FLCN specifically binds to one or many small GTPases in a nucleotide-specific fashion. Moreover, due to the fact that FNIP1 and FNIP2 were only identified as minor binding partners, it may be valuable to perform immunoaffinity enrichments with these proteins and identify their unique functional interactions, if any truly exist. While out of the scope of this work, these novel future studies would also identify and support existing knowledge into FLCN interactions and elucidate core FLCN-FNIP1-FNIP2 complexes.



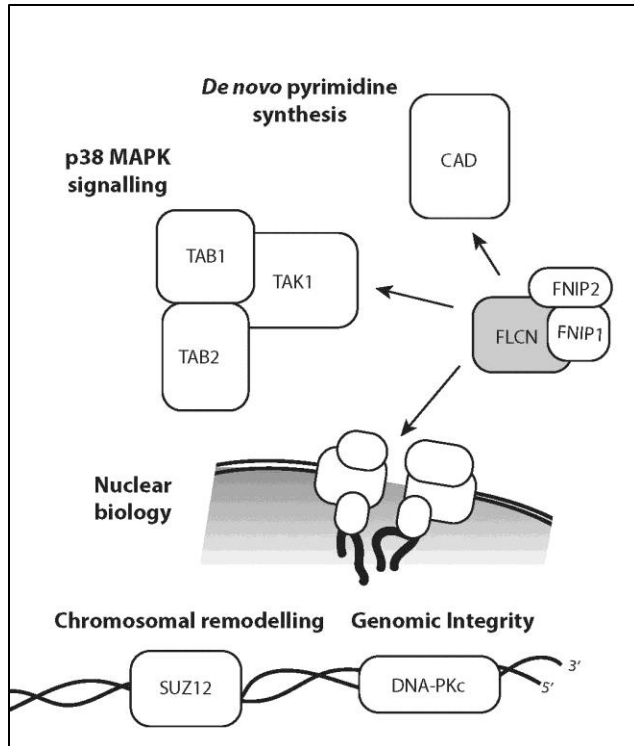
## 5. Summary of research highlights

1) Characterisation of a novel ULK1 inhibitor—a limitation in the autophagy field has been a lack of a drug inhibitor of ULK1 and initiating kinases. Consequently, this new drug, QG000052, will be of considerable interest to the autophagy community. The validation of its specificity and temporal response is further support for its use in other models.



2) Identification of new ULK1 protein interactions involved in fundamental processes of autophagy including PIKfyve/Vac14, which is critically involved in autosomal maturation from the ER and subsequent translocation to the lysosome, support new avenues of research and a better understanding of the complex, dynamic biological process.

3) Identification of disparity between human ULK1 and *S. cerevisiae* atg1 targets highlights distinct and shared targets, and further support to study autophagy to a greater extent in human cell lines.



4) Better characterisation of a poorly understood substrate of ULK1, FLCN, which is linked to mTORC1 and AMPK signalling. By carrying out unbiased FLCN interactions, many new mechanisms of FLCN function have been uncovered (as well as to validate it as an ULK1 interactor) that is directly linked to the cilia and renal cell carcinoma involving energy metabolism and DNA damage.

## 6. References

1. Behrends, C., et al., *Network organization of the human autophagy system*. Nature, 2010. **466**(7302): p. 68-76.
2. Russell, R.C., H.X. Yuan, and K.L. Guan, *Autophagy regulation by nutrient signaling*. Cell Res, 2014. **24**(1): p. 42-57.
3. Kabeya, Y., et al., *LC3, GABARAP and GATE16 localize to autophagosomal membrane depending on form-II formation*. J Cell Sci, 2004. **117**(Pt 13): p. 2805-12.
4. Tanida, I., et al., *The human homolog of Saccharomyces cerevisiae Apg7p is a Protein-activating enzyme for multiple substrates including human Apg12p, GATE-16, GABARAP, and MAP-LC3*. J Biol Chem, 2001. **276**(3): p. 1701-6.
5. Cheong, H., et al., *Analysis of a lung defect in autophagy-deficient mouse strains*. Autophagy, 2014. **10**(1): p. 45-56.
6. Takamura, A., et al., *Autophagy-deficient mice develop multiple liver tumors*. Genes Dev, 2011. **25**(8): p. 795-800.
7. Eskelinen, E.L., *The dual role of autophagy in cancer*. Curr Opin Pharmacol, 2011. **11**(4): p. 294-300.
8. Yang, S.Y. and M.C. Winslet, *Dual role of autophagy in colon cancer cell survival*. Ann Surg Oncol, 2011. **18 Suppl 3**: p. S239.
9. Pike, L.R., et al., *Transcriptional up-regulation of ULK1 by ATF4 contributes to cancer cell survival*. Biochem J, 2013. **449**(2): p. 389-400.
10. Rao, S., et al., *A dual role for autophagy in a murine model of lung cancer*. Nat Commun, 2014. **5**: p. 3056.

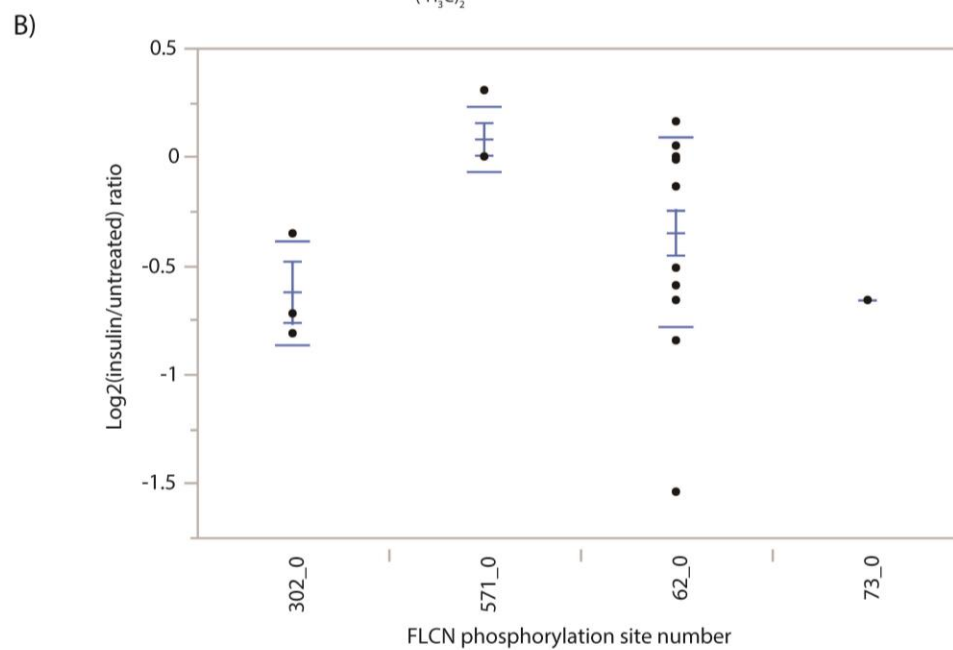
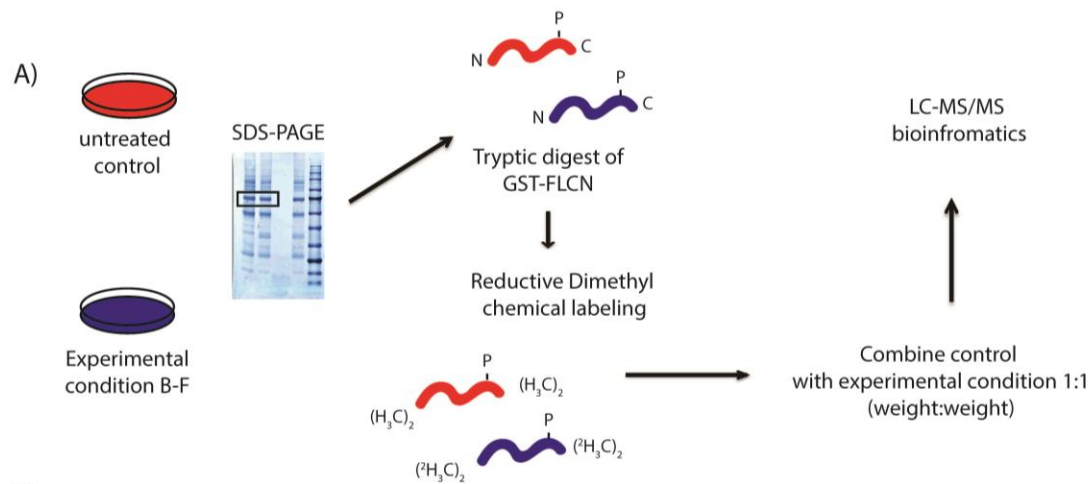
11. Papinski, D., et al., *Early steps in autophagy depend on direct phosphorylation of Atg9 by the Atg1 kinase*. Mol Cell, 2014. **53**(3): p. 471-83.
12. Puri, C., et al., *ATG16L1 meets ATG9 in recycling endosomes: additional roles for the plasma membrane and endocytosis in autophagosome biogenesis*. Autophagy, 2014. **10**(1): p. 182-4.
13. Mercer, C.A., A. Kaliappan, and P.B. Dennis, *A novel, human Atg13 binding protein, Atg101, interacts with ULK1 and is essential for macroautophagy*. Autophagy, 2009. **5**(5): p. 649-62.
14. McAlpine, F., et al., *Regulation of nutrient-sensitive autophagy by uncoordinated 51-like kinases 1 and 2*. Autophagy, 2013. **9**(3): p. 361-73.
15. Lazarus, M.B., C.J. Novotny, and K.M. Shokat, *Structure of the human autophagy initiating kinase ULK1 in complex with potent inhibitors*. ACS Chem Biol, 2015. **10**(1): p. 257-61.
16. Chan, E.Y., et al., *Kinase-inactivated ULK proteins inhibit autophagy via their conserved C-terminal domains using an Atg13-independent mechanism*. Mol Cell Biol, 2009. **29**(1): p. 157-71.
17. Egan, D.F., et al., *Phosphorylation of ULK1 (hATG1) by AMP-activated protein kinase connects energy sensing to mitophagy*. Science, 2011. **331**(6016): p. 456-61.
18. Kim, J., et al., *AMPK and mTOR regulate autophagy through direct phosphorylation of Ulk1*. Nat Cell Biol, 2011. **13**(2): p. 132-41.
19. Kim, J. and K.L. Guan, *Regulation of the autophagy initiating kinase ULK1 by nutrients: roles of mTORC1 and AMPK*. Cell Cycle, 2011. **10**(9): p. 1337-8.
20. Nazio, F., et al., *mTOR inhibits autophagy by controlling ULK1 ubiquitylation, self-association and function through AMBRA1 and TRAF6*. Nat Cell Biol, 2013. **15**(4): p. 406-16.
21. Dunlop, E.A., et al., *FLCN, a novel autophagy component, interacts with GABARAP and is regulated by ULK1 phosphorylation*. Autophagy, 2014. **10**(10): p. 1749-60.
22. Loffler, A.S., et al., *Ulk1-mediated phosphorylation of AMPK constitutes a negative regulatory feedback loop*. Autophagy, 2011. **7**(7): p. 696-706.
23. Russell, R.C., et al., *ULK1 induces autophagy by phosphorylating Beclin-1 and activating VPS34 lipid kinase*. Nat Cell Biol, 2013. **15**(7): p. 741-50.
24. Di Bartolomeo, S., et al., *The dynamic interaction of AMBRA1 with the dynein motor complex regulates mammalian autophagy*. J Cell Biol, 2010. **191**(1): p. 155-68.
25. Hasumi, Y., et al., *Homozygous loss of BHD causes early embryonic lethality and kidney tumor development with activation of mTORC1 and mTORC2*. Proc Natl Acad Sci U S A, 2009. **106**(44): p. 18722-7.
26. Piao, X., et al., *Regulation of folliculin (the BHD gene product) phosphorylation by Tsc2-mTOR pathway*. Biochem Biophys Res Commun, 2009. **389**(1): p. 16-21.
27. van Steensel, M.A., et al., *Novel mutations in the BHD gene and absence of loss of heterozygosity in fibrofolliculomas of Birt-Hogg-Dube patients*. J Invest Dermatol, 2007. **127**(3): p. 588-93.
28. Baba, M., et al., *Folliculin encoded by the BHD gene interacts with a binding protein, FNIP1, and AMPK, and is involved in AMPK and mTOR signaling*. Proc Natl Acad Sci U S A, 2006. **103**(42): p. 15552-7.
29. Tsun, Z.Y., et al., *The folliculin tumor suppressor is a GAP for the RagC/D GTPases that signal amino acid levels to mTORC1*. Mol Cell, 2013. **52**(4): p. 495-505.

30. Petit, C.S., A. Roczniak-Ferguson, and S.M. Ferguson, *Recruitment of folliculin to lysosomes supports the amino acid-dependent activation of Rag GTPases*. J Cell Biol, 2013. **202**(7): p. 1107-22.
31. Yan, M., et al., *The tumor suppressor folliculin regulates AMPK-dependent metabolic transformation*. J Clin Invest, 2014. **124**(6): p. 2640-50.
32. Preston, R.S., et al., *Absence of the Birt-Hogg-Dube gene product is associated with increased hypoxia-inducible factor transcriptional activity and a loss of metabolic flexibility*. Oncogene, 2011. **30**(10): p. 1159-73.
33. Medvetz, D.A., et al., *Folliculin, the product of the Birt-Hogg-Dube tumor suppressor gene, interacts with the adherens junction protein p0071 to regulate cell-cell adhesion*. PLoS One, 2012. **7**(11): p. e47842.
34. Luijten, M.N., et al., *Birt-Hogg-Dube syndrome is a novel ciliopathy*. Hum Mol Genet, 2013. **22**(21): p. 4383-97.
35. Ong, S.E., et al., *Stable isotope labeling by amino acids in cell culture, SILAC, as a simple and accurate approach to expression proteomics*. Mol Cell Proteomics, 2002. **1**(5): p. 376-86.
36. Elias, J.E. and S.P. Gygi, *Target-decoy search strategy for increased confidence in large-scale protein identifications by mass spectrometry*. Nat Methods, 2007. **4**(3): p. 207-14.
37. Beausoleil, S.A., et al., *A probability-based approach for high-throughput protein phosphorylation analysis and site localization*. Nat Biotechnol, 2006. **24**(10): p. 1285-92.
38. Koyama-Honda, I., et al., *Temporal analysis of recruitment of mammalian ATG proteins to the autophagosome formation site*. Autophagy, 2013. **9**(10): p. 1491-9.
39. Holland, P., et al., *LYST affects lysosome size and quantity, but not trafficking or degradation through autophagy or endocytosis*. Traffic, 2014. **15**(12): p. 1390-405.
40. Rahman, M., et al., *Drosophila mauve mutants reveal a role of LYST homologs late in the maturation of phagosomes and autophagosomes*. Traffic, 2012. **13**(12): p. 1680-92.
41. Zhang, J., et al., *Rabankyrin-5 interacts with EHD1 and Vps26 to regulate endocytic trafficking and retromer function*. Traffic, 2012. **13**(5): p. 745-57.
42. Pieren, M., A. Schmidt, and A. Mayer, *The SM protein Vps33 and the t-SNARE H(abc) domain promote fusion pore opening*. Nat Struct Mol Biol, 2010. **17**(6): p. 710-7.
43. Inoue, H., et al., *Arf GTPase-activating protein ASAP1 interacts with Rab11 effector FIP3 and regulates pericentrosomal localization of transferrin receptor-positive recycling endosome*. Mol Biol Cell, 2008. **19**(10): p. 4224-37.
44. Popovic, D., et al., *Rab GTPase-activating proteins in autophagy: regulation of endocytic and autophagy pathways by direct binding to human ATG8 modifiers*. Mol Cell Biol, 2012. **32**(9): p. 1733-44.
45. Wang, J., et al., *The Arf GAP ASAP1 provides a platform to regulate Arf4- and Rab11-Rab8-mediated ciliary receptor targeting*. EMBO J, 2012. **31**(20): p. 4057-71.
46. Dummler, B.A., et al., *Functional characterization of human RSK4, a new 90-kDa ribosomal S6 kinase, reveals constitutive activation in most cell types*. J Biol Chem, 2005. **280**(14): p. 13304-14.

47. Ikonomov, O.C., et al., *Functional dissection of lipid and protein kinase signals of PIKfyve reveals the role of PtdIns 3,5-P2 production for endomembrane integrity.* J Biol Chem, 2002. **277**(11): p. 9206-11.
48. Dunlop, E.A., et al., *ULK1 inhibits mTORC1 signaling, promotes multisite Raptor phosphorylation and hinders substrate binding.* Autophagy, 2011. **7**(7): p. 737-47.
49. Hsu, P.P., et al., *The mTOR-regulated phosphoproteome reveals a mechanism of mTORC1-mediated inhibition of growth factor signaling.* Science, 2011. **332**(6035): p. 1317-22.
50. Polson, H.E., et al., *Mammalian Atg18 (WIPI2) localizes to omegasome-anchored phagophores and positively regulates LC3 lipidation.* Autophagy, 2010. **6**(4): p. 506-22.
51. Zhu, G., et al., *Exceptional disfavor for proline at the P + 1 position among AGC and CAMK kinases establishes reciprocal specificity between them and the proline-directed kinases.* J Biol Chem, 2005. **280**(11): p. 10743-8.
52. Ubersax, J.A. and J.E. Ferrell, Jr., *Mechanisms of specificity in protein phosphorylation.* Nat Rev Mol Cell Biol, 2007. **8**(7): p. 530-41.
53. Elia, A.E., L.C. Cantley, and M.B. Yaffe, *Proteomic screen finds pSer/pThr-binding domain localizing Plk1 to mitotic substrates.* Science, 2003. **299**(5610): p. 1228-31.
54. Ben-Sahra, I., et al., *Stimulation of de novo pyrimidine synthesis by growth signaling through mTOR and S6K1.* Science, 2013. **339**(6125): p. 1323-8.
55. Sato, T., et al., *Rheb protein binds CAD (carbamoyl-phosphate synthetase 2, aspartate transcarbamoylase, and dihydroorotase) protein in a GTP- and effector domain-dependent manner and influences its cellular localization and carbamoyl-phosphate synthetase (CPSase) activity.* J Biol Chem, 2015. **290**(2): p. 1096-105.
56. D'Assoro, A.B., et al., *The mitotic kinase Aurora-a promotes distant metastases by inducing epithelial-to-mesenchymal transition in ERalpha(+) breast cancer cells.* Oncogene, 2014. **33**(5): p. 599-610.
57. Baude, A., A.M. Lindroth, and C. Plass, *PRC2 loss amplifies Ras signaling in cancer.* Nat Genet, 2014. **46**(11): p. 1154-5.
58. Brecqueville, M., et al., *Mutation analysis of ASXL1, CBL, DNMT3A, IDH1, IDH2, JAK2, MPL, NF1, SF3B1, SUZ12, and TET2 in myeloproliferative neoplasms.* Genes Chromosomes Cancer, 2012. **51**(8): p. 743-55.
59. De Raedt, T., et al., *PRC2 loss amplifies Ras-driven transcription and confers sensitivity to BRD4-based therapies.* Nature, 2014. **514**(7521): p. 247-51.
60. Pasini, D., et al., *The polycomb group protein Suz12 is required for embryonic stem cell differentiation.* Mol Cell Biol, 2007. **27**(10): p. 3769-79.
61. Seo, S., et al., *BBS6, BBS10, and BBS12 form a complex with CCT/TRiC family chaperonins and mediate BBSome assembly.* Proc Natl Acad Sci U S A, 2010. **107**(4): p. 1488-93.
62. Plotnikova, O.V., et al., *INPP5E interacts with AURKA, linking phosphoinositide signaling to primary cilium stability.* J Cell Sci, 2015. **128**(2): p. 364-72.
63. Plotnikova, O.V., et al., *Calmodulin activation of Aurora-A kinase (AURKA) is required during ciliary disassembly and in mitosis.* Mol Biol Cell, 2012. **23**(14): p. 2658-70.
64. Kasahara, K., et al., *Ubiquitin-proteasome system controls ciliogenesis at the initial step of axoneme extension.* Nat Commun, 2014. **5**: p. 5081.

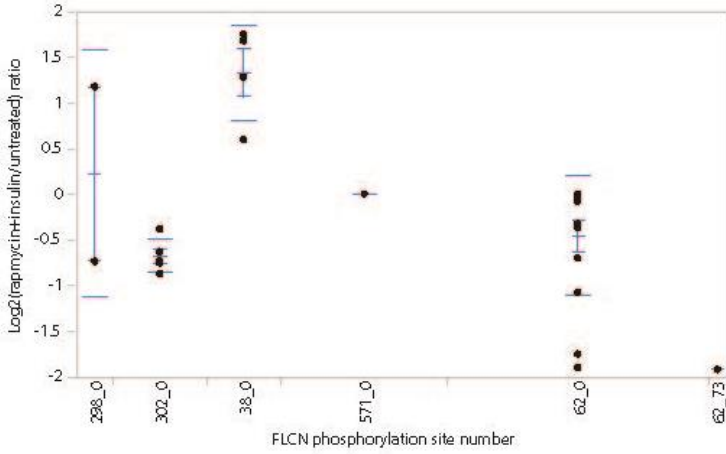
65. Liu, Y.P., et al., *Ciliopathy proteins regulate paracrine signaling by modulating proteasomal degradation of mediators*. J Clin Invest, 2014. **124**(5): p. 2059-70.
66. Orhon, I., et al., *Autophagy and regulation of cilia function and assembly*. Cell Death Differ, 2015. **22**(3): p. 389-97.
67. Kee, H.L., et al., *A size-exclusion permeability barrier and nucleoporins characterize a ciliary pore complex that regulates transport into cilia*. Nat Cell Biol, 2012. **14**(4): p. 431-7.
68. Marat, A.L., H. Dokainish, and P.S. McPherson, *DENN domain proteins: regulators of Rab GTPases*. J Biol Chem, 2011. **286**(16): p. 13791-800.
69. Hong, S.B., et al., *Tumor suppressor FLCN inhibits tumorigenesis of a FLCN-null renal cancer cell line and regulates expression of key molecules in TGF-beta signaling*. Mol Cancer, 2010. **9**: p. 160.
70. Senftleben, U., et al., *Activation by IKKalpha of a second, evolutionary conserved, NF-kappa B signaling pathway*. Science, 2001. **293**(5534): p. 1495-9.
71. Dolcet, X., et al., *Proteasome inhibitors induce death but activate NF-kappaB on endometrial carcinoma cell lines and primary culture explants*. J Biol Chem, 2006. **281**(31): p. 22118-30.
72. Morais, C., et al., *The emerging role of nuclear factor kappa B in renal cell carcinoma*. Int J Biochem Cell Biol, 2011. **43**(11): p. 1537-49.
73. Haskill, S., et al., *Characterization of an immediate-early gene induced in adherent monocytes that encodes I kappa B-like activity*. Cell, 1991. **65**(7): p. 1281-9.
74. Hacker, H. and M. Karin, *Regulation and function of IKK and IKK-related kinases*. Sci STKE, 2006. **2006**(357): p. re13.
75. Nahorski, M.S., et al., *Birt Hogg-Dube syndrome-associated FLCN mutations disrupt protein stability*. Hum Mutat, 2011. **32**(8): p. 921-9.
76. Pampliega, O., et al., *Functional interaction between autophagy and ciliogenesis*. Nature, 2013. **502**(7470): p. 194-200.
77. Angers, S. and R.T. Moon, *Proximal events in Wnt signal transduction*. Nat Rev Mol Cell Biol, 2009. **10**(7): p. 468-77.
78. Cervantes, S., et al., *Primary cilia regulate Gli/Hedgehog activation in pancreas*. Proc Natl Acad Sci U S A, 2010. **107**(22): p. 10109-14.
79. Han, Y.G., et al., *Hedgehog signaling and primary cilia are required for the formation of adult neural stem cells*. Nat Neurosci, 2008. **11**(3): p. 277-84.
80. Wilson, C.W. and D.Y. Stainier, *Vertebrate Hedgehog signaling: cilia rule*. BMC Biol, 2010. **8**: p. 102.

## **Supplemental Figures**

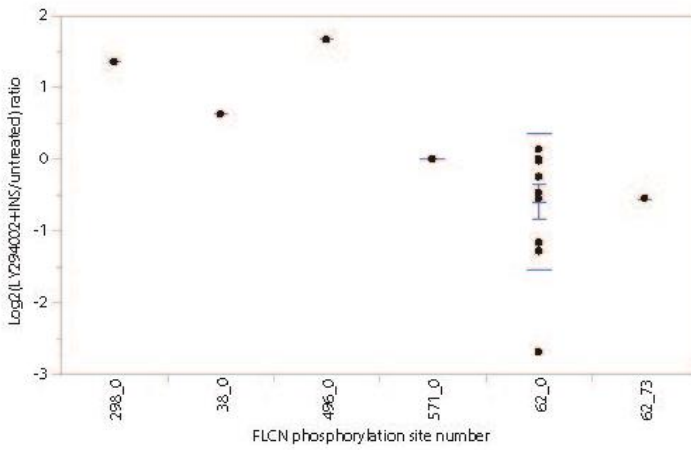


Level	Number	Mean	Std Dev	Std Err		
				Mean	Lower 95%	Upper 95%
298_0	2	-0.1552	1.40397	0.99276	-12.77	12.46
302_0	1	-1.1479	.	.	.	.
38_0	2	1.3198	0.00000	0.00000	1.32	1.32
571_0	9	-0.0015	0.00438	0.00146	-0.0048	0.00191
62_0	17	-0.3077	0.33133	0.08036	-0.48	-0.14
62_73	1	-0.6540	.	.	.	.

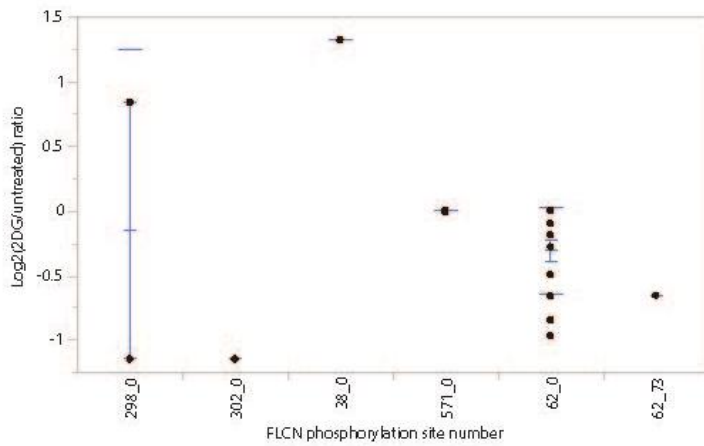




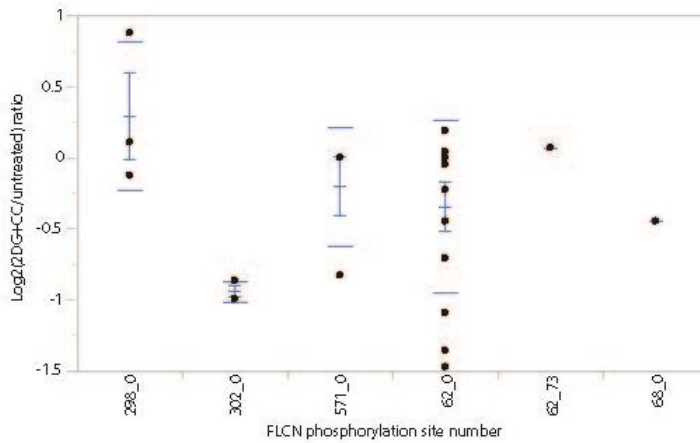
Level	Number	Mean	Std Dev	Std Err		
				Mean	Lower 95%	Upper 95%
298_0	2	0.2157	1.35169	0.95579	-11.93	12.36
302_0	5	-0.6778	0.18378	0.08219	-0.91	-0.45
38_0	4	1.3236	0.52968	0.26484	0.48	2.17
571_0	9	0.0000	0.00000	0.00000	0.00	0.00
62_0	14	-0.4639	0.65739	0.17569	-0.84	-0.0844
62_73	1	-1.9248	.	.	.	.



Level	Number	Mean	Std Dev	Std Err		
				Mean	Lower 95%	Upper 95%
298_0	1	1.3564	.	.	.	.
38_0	1	0.6203	.	.	.	.
496_0	1	1.6592	.	.	.	.
571_0	5	0.0000	0.000000	0.00000	0.000	0.0000
62_0	15	-0.6078	0.960546	0.24801	-1.140	-0.0759
62_73	1	-0.5521	.	.	.	.



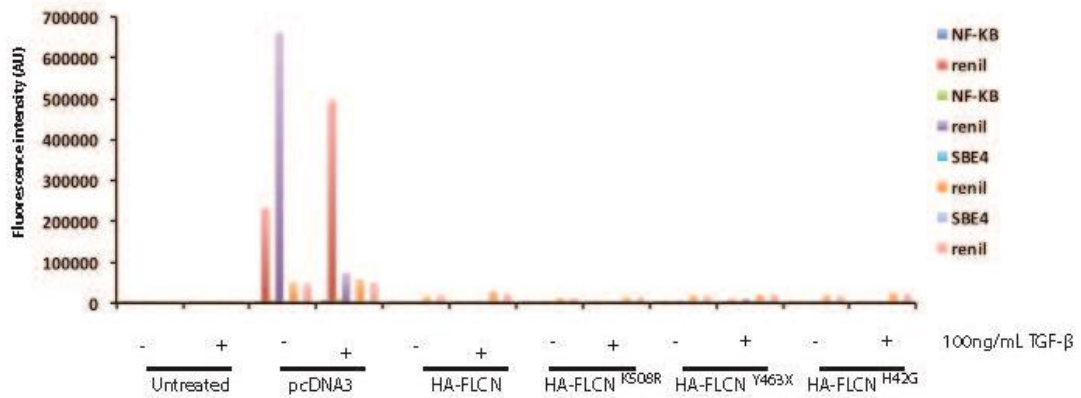
Level	Number	Mean	Std Dev	Std Err		
				Mean	Lower 95%	Upper 95%
298_0	2	-0.1552	1.40397	0.99276	-12.77	12.46
302_0	1	-1.1479	.	.	.	.
38_0	2	1.3198	0.00000	0.00000	1.32	1.32
571_0	9	-0.0015	0.00438	0.00146	-0.0048	0.00191
62_0	17	-0.3077	0.33133	0.08036	-0.48	-0.14
62_73	1	-0.6540	.	.	.	.



Level	Number	Mean	Std Dev	Std Err		
				Mean	Lower 95%	Upper 95%
298_0	3	0.28674	0.524439	0.30279	-1.016	1.590
302_0	3	-0.95137	0.072824	0.04205	-1.132	-0.770
571_0	4	-0.20726	0.414520	0.20726	-0.867	0.452
62_0	13	-0.35046	0.613062	0.17003	-0.721	0.020
62_73	1	0.06752	.	.	.	.
68_0	1	-0.44764	.	.	.	.

**Supplemental Figure S1. Quantification of chemically labelled, phosphorylated FLCN peptides under pharmacological inhibitor treatment.**

A) To determine how cell treatments effected FLCN phosphorylation status chemically labeled peptides were combined so the ratio of treated:untreated samples was 1:1 (*wt/wt*). HK2 cells over-expressing FLCN were treated with B) insulin, C) insulin and rapamycin, D) insulin and LY294002, E) 2-deoxy-glucose, or, F) 2-deoxy-glucose and compound C and quantitatively compared to an untreated control condition. High-resolution quantitative mass spectrometry was used to resolve the mass difference between treated and untreated peptides and quantification was performed by comparing the relative difference in abundance of isotopically-labelled heavy and light precursor masses. The identified phosphorylation site number, treatment, and identification statistics are provided. The full list of FLCN phosphorylation sites from this experiment can be found in Supplemental Table S8.



**Supplemental Figure S2. Luciferase assay measurements to detect the role of FLCN mutation in NF-κB and TGF-β signalling response.**

HK2 cells depleted of endogenous FLCN were transfected transiently with cDNA to pCDNA3, HA-FLCN, HA-FLCN<sup>K508R</sup>, HA-FLCN<sup>Y463X</sup>, or HA-FLCN<sup>H42G</sup> and either an NF-κB or SMAD reporter construct with a renilla control for transfection efficiency in a 96-well plate. Following transfection, cells were supplemented with 1ng/mL of TGF-β or mock treated with water. Fluorescence of reporter and transfection control constructs was visualized on a plate reader 6 hours after stimulation.

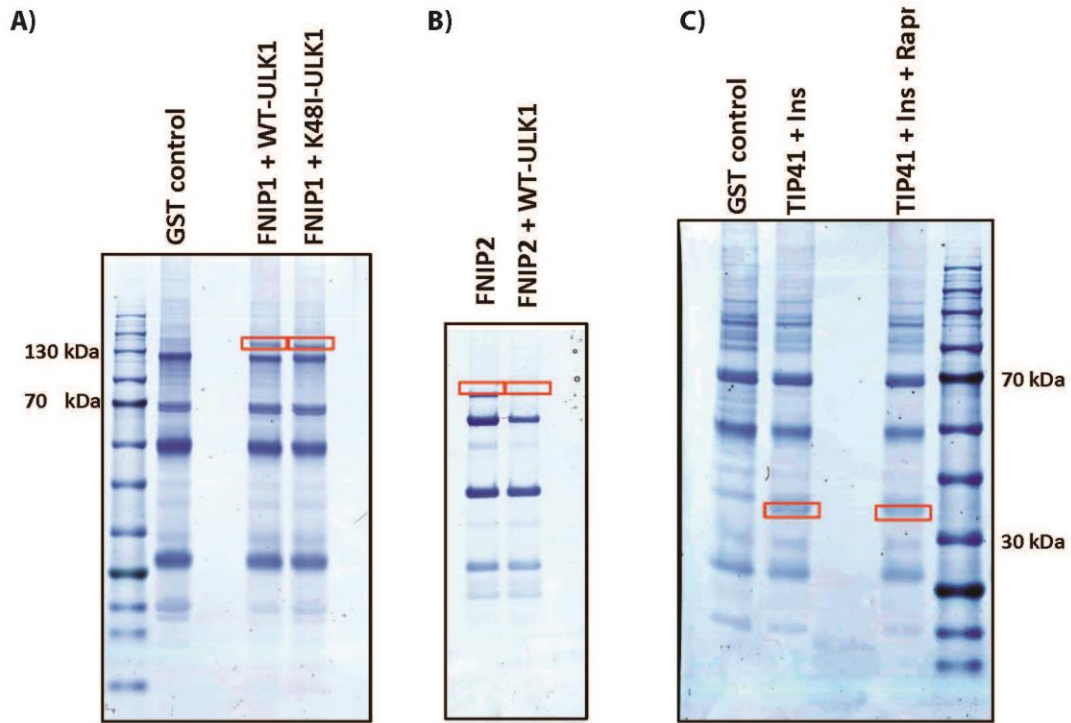
```

sp | Q8TEH3 | DEN1A_HUMAN | -----MGSRIKQNPETTFEVYVEVAYPRTGGTLDPEVQRQFPEDYSD 43
sp | Q6P3S1 | DEN1B_HUMAN | -----MDCRTKANPDRTFDLVLKVKCHAS--ENEDPVVLWKFPEDFGD 41
sp | Q8NFG4 | FLCN_HUMAN | MNAIVALCHFCELHGPRTLFCFEVLHAPLPQGDGNEDSPGQGEQAEIEEEG 50
      * * : * * : * * : * * :
sp | Q8TEH3 | DEN1A_HUMAN | QEVLQTLTKFCFPFYVDSLTVSQVGNFTFVLTLDIDSKQRFGFCRLSSGA 93
sp | Q6P3S1 | DEN1B_HUMAN | QEILQSVPKFCFPFDVERVSQNVGQHFTFVLTLDIESKQRFGFCRLTSSG 91
sp | Q8NFG4 | FLCN_HUMAN | GIQMNSRMRRAHSPAEGASVESSPGP-----KSDMCEGCRSLAAGH 92
      : : * : * * * * * * * * * *
sp | Q8TEH3 | DEN1A_HUMAN | KSCFCILSYLPWFVEVYKLLNLADYTKRQENQWNELETLHKLPIPD 143
sp | Q6P3S1 | DEN1B_HUMAN | TICLCILSYLPWFVEVYKLLNLADYLAKELENDLNETLRSLYNHPVKA 141
sp | Q8NFG4 | FLCN_HUMAN | PGIYSHDKETS IKYVSHQHPSHPQLFSIVR-----QACVRSLSCEVCPGR 137
      : . . * * : : . . : : * * *
sp | Q8TEH3 | DEN1A_HUMAN | GVSVHLSV-----HSYFTVPDTRELPSIPENRNLT 173
sp | Q6P3S1 | DEN1B_HUMAN | NTPVNLNVNQEIFIACEQVLKQDPALVPHSYF IAPDVTGLPTIPESRNLT 191
sp | Q8NFG4 | FLCN_HUMAN | EGP IFFGDEQ-----HGFVFSHTFFIKDSLARGPQRW 169
      . : . * . . * . . . : : . :
sp | Q8TEH3 | DEN1A_HUMAN | EYFVAVDVNNMLHLYASMLYERRILICSKLSTLTACIHGSAAMLYPMW 223
sp | Q6P3S1 | DEN1B_HUMAN | EYFVAVDVNNMLQLYASMLHERRIVIISSKLSLTACIHGSAALLYPMW 241
sp | Q8NFG4 | FLCN_HUMAN | YSIIITIMDRIYLINSWPFLLGKVRGIIDELQKALKVFEEQFGCPQRA 219
      : : : : : : : : : : * . : * : : : : *
sp | Q8TEH3 | DEN1A_HUMAN | QHVYIPVLPPLLDDYCCAMPYLGIIHLSLMEKVRNMLDDVVILNVDTN 273
sp | Q6P3S1 | DEN1B_HUMAN | QHIYIPVLPPLLDDYCCAMPYLGIIHSLIERVKNKSLLEDVVMNVDTN 291
sp | Q8NFG4 | FLCN_HUMAN | QRMNTAFTP-----FLHQRNNGNAARSLTSLTSDDN 249
      * : : . * * : : . : : . : * * *
sp | Q8TEH3 | DEN1A_HUMAN | TLETFFDDLQSLPNDVISSLKNRLKVVSTTGDGVARAFKAQAAPFGSY 323
sp | Q6P3S1 | DEN1B_HUMAN | TLESFFSDLNLPDVSALKNKLKQSTATGDGVARAFRAQAALFGSY 341
sp | Q8NFG4 | FLCN_HUMAN | LWACLHTSFAWLLKACGSRLETKLELLEGAPTE TLVQMEKLADLEEESES 299
      . : * * * * : : : . * * * *
sp | Q8TEH3 | DEN1A_HUMAN | RNALKIEPEEPIITFCEEAFVSHYRSGAMRQFLQN---ATQLQLFKQFIDG 370
sp | Q6P3S1 | DEN1B_HUMAN | RDALRYKPGEPITFCEESFVKH-RSSVMKQFLET---AINLQLFKQFIDG 387
sp | Q8NFG4 | FLCN_HUMAN | DNSEAEIEEEKAPVLPPESTEGREL TQGAESSLSGCGSWQPRKLPVFKSL 349
      : : : : * . : . . . . : : : * .
sp | Q8TEH3 | DEN1A_HUMAN | RLDLLNSGEGFSDVFEEINMGYAGSDKLYHQWLS TVRKSGGAILNTVK 420
sp | Q6P3S1 | DEN1B_HUMAN | RLAKLNAGRGFSDVFEEITSGGFCG----- 413
sp | Q8NFG4 | FLCN_HUMAN | RHMRQVLGAPSFRLAWHVLGMGNQVIWK----- 377
      * * : : *
sp | Q8TEH3 | DEN1A_HUMAN | TKANPAMKTVYKFAKDHA MG I KEVNRLKQKDAENGCAPTPEEQPKT 470
sp | Q6P3S1 | DEN1B_HUMAN | --GKDKLQYDYFFSQ----- 426
sp | Q8NFG4 | FLCN_HUMAN | SRDVDLVQSAFEVLR TMLPVGCVRIIPYSSQYEEAYR-----CNFL 418
      : : : . :
sp | Q8TEH3 | DEN1A_HUMAN | APSPLVEAKDKLREDRRPITVHFGQVRPPRHVVKRPKSNIAVEGRRTS 520
sp | Q6P3S1 | DEN1B_HUMAN | ----- 453
sp | Q8NFG4 | FLCN_HUMAN | GLSPHVQIPPHVLSSEFAVIVEVHAAARSTLHPVG----- 453
sp | Q8TEH3 | DEN1A_HUMAN | VPSPEQPQPYRTLRESDSAEGDEAESPEQQVRKSTGFPVPAPPDRAASIDL 570
sp | Q6P3S1 | DEN1B_HUMAN | ----- 485
sp | Q8NFG4 | FLCN_HUMAN | -----CEDDQSLSKYEFVVTSGSPVAADRVGPTILNK 485
sp | Q8TEH3 | DEN1A_HUMAN | LEDVFSNLDMEAAQLPLGQAKSLEDLRAPKDLREQPGTFDYQRLDLGGSE 620
sp | Q6P3S1 | DEN1B_HUMAN | ----- 530
sp | Q8NFG4 | FLCN_HUMAN | IEAALTNQNSVDVVDQCLVCLKEEWMN----KVKVLFKFTKVDSRPKE 530

```

**Supplemental Figure S3. Multiple sequence alignment of FLCN and DEN1A and DEN1B highlights DENN-like domain in FLCN.**

Full length FLCN (Q8NFG4), DEN1A (Q8TEH3) and DEN1B (Q6P3S1) were analyzed for sequence similarity using the ClustalW2 multiple sequence alignment software (<http://www.ebi.ac.uk/Tools/msa/clustalw2>). Identity is denoted by (\*) and similarity by (: ) and (.).



**D)**

Protein	P-sites	Experiment	# peptides
FNIP1	220	FNIP1 + ULK1	2
FNIP1	296	FNIP1 + ULK1	1
FNIP1	487	FNIP1 + ULK1	1
FNIP1	769	FNIP1 + ULK1	1
FNIP1	846	FNIP1 + ULK1	2
FNIP1	987	FNIP1 + ULK1	2
FNIP1	1099	FNIP1 + ULK1-K48I	1
FNIP1	220	FNIP1 + ULK1-K48I	1
FNIP1	760	FNIP1 + ULK1-K48I	3
FNIP1	946	FNIP1 + ULK1-K48I	4



E)

Protein	P-site	Experiment	# peptides
FNIP2	1000	FNIP2	3
<b>FNIP2</b>	<b>285</b>	<b>FNIP2</b>	<b>1</b>
<b>FNIP2</b>	<b>298</b>	<b>FNIP2</b>	<b>1</b>
<b>FNIP2</b>	<b>300</b>	<b>FNIP2</b>	<b>1</b>
<b>FNIP2</b>	<b>357</b>	<b>FNIP2</b>	<b>1</b>
FNIP2	677	FNIP2	4
FNIP2	726	FNIP2	2
<b>FNIP2</b>	<b>733</b>	<b>FNIP2</b>	<b>1</b>
<b>FNIP2</b>	<b>748, 752</b>	<b>FNIP2</b>	<b>2</b>
<b>FNIP2</b>	<b>766</b>	<b>FNIP2</b>	<b>2</b>
<b>FNIP2</b>	<b>954</b>	<b>FNIP2</b>	<b>1</b>
FNIP2	1000	FNIP2 + ULK1	2
FNIP2	208	FNIP2 + ULK1	1
FNIP2	221	FNIP2 + ULK1	3
FNIP2	287	FNIP2 + ULK1	2
FNIP2	469	FNIP2 + ULK1	1
FNIP2	677	FNIP2 + ULK1	1
FNIP2	726	FNIP2 + ULK1	2

F)

Protein	P-sites	Experiment	# peptides
TIP41	199, 202	TIP41 + INS	1
<b>TIP41</b>	<b>265</b>	<b>TIP41 + INS</b>	<b>2</b>
TIP41	199, 202	TIP41 + RAP + INS	1
<b>TIP41</b>	<b>96</b>	<b>TIP41 + RAP + INS</b>	<b>1</b>

**Supplemental Figure S4. Identification of FNIP1, FNIP2 and TIP41 phosphorylation sites.** A-C) Following pull-down of GST-FNIP1, GST-FNIP2 and GST-TIP41, bands corresponding to within a 10kDa window of each protein's molecular weight was excised and processed for analysis by mass spectrometry. D-F) Phosphorylation sites from each protein and experimental condition were identified by high-resolution mass spectrometry. Unique phosphorylation sites that do not overlap between treatment and control conditions are provided in bold, and the gene, experimental treatment, total number of phosphopeptides identified and phosphorylation site number (uniprot numbering) are provided for each protein.